Ore Geology Reviews 101 (2018) 652–674

Contents lists available at ScienceDirect

Ore Geology Reviews

journal homepage: www.elsevier.com/locate/oregeorev

Geology and geochemistry of sediment-hosted Hanönü massive sulfide deposit (Kastamonu – Turkey)

Kurtuluş Günay[a,*], Cahit Dönmez[a], Vural Oyan[b], Nail Yıldırım[a], Emin Çiftçi[c], Hayrullah Yıldız[a], Serkan Özkümüş[a]

[a] General Directorate of Mineral Research and Exploration, Department of Mineral Research and Exploration, Ankara, Turkey
[b] Van Yüzüncü Yıl University, Department of Mining Engineering, Van, Turkey
[c] İstanbul Technical University, Department of Geological Engineering, İstanbul, Turkey

ARTICLE INFO

Keywords:
Massive sulphide
Mafic volcanics
Tethyan
Hanönü VMS deposit
Besshi-type

ABSTRACT

Hanönü massive sulfide (HMS) mineralization is the first sediment-hosted massive sulfide deposit discovered in Anatolia (Turkey). Containing more than 1% Cu and with more than 25 million tonnes reserve, the HMS mineralization is located in the Çangaldağ Metamorphic Complex (CMC) in the central Pontides within metavolcaniclastic rocks with mafic sill and/or lava interlayers. Rocks related to mineralization were exposed to metamorphism under the greenschist facies conditions. Tectonism and metamorphic processes affected all units including ore. The HMS mineralization consists dominantly of Cu (0.2–6.9%) accompanied by Zn (239 ppm–1%) and comprises massive, banded and disseminated sulfide bodies. The main ore minerals include pyrite, chalcopyrite, with minor sphalerite and magnetite. The regular stratigraphy displaying uninterrupted layers of volcanoclastics contains mafic lava or sills within the sequence with the mineralization initially emplaced within immature clastics and then subjected to metamorphism as a package, which indicates that the ore and wall rocks formed in the same paleotectonic environment. Data obtained from melt models of mafic lava or sills related to the HMS mineralization indicate these rocks formed in back-arc basins from a mixture of 70% depleted MORB mantle and 30% asthenospheric melt with melting degrees possibly of 8–15%. According to isotope data, lead from the HMS mineralization may be sourced from an arc-related environment, with magmatic activity in the lower crust and upper mantle. Geologic and geochemical data indicate that the HMS mineralization may have formed in a back-arc rift tectonomagmatic environment.

1. Introduction

Volcanogenic massive sulfide deposits (VMS) are one of the most important sources for base metal sulfides (copper, zinc, lead) (Mosier et al., 1983). Nearly 1100 massive sulfide deposits are known globally, with the majority on the American continent (Mosier et al., 1983; Galley et al., 2007). Massive sulfide deposits have high grade, generally Fe-Mg oxyhydroxide/gossan sections at the surface, clear contacts with wall rocks and relatively simple processing characteristics, as such they are among the oldest metallic mineral deposits discovered. In this way, massive sulfides have formed the basis of many scientific research articles, and are a metallic mineral deposit type with a significant amount of data available (Franklin et al., 1981; Fox, 1984; Goodfellow and Franklin, 1993; Humphris et al., 1995; Ohmoto, 1996; Hannington et al., 1999; Goodfellow et al., 2003; Galley et al., 2007; Piercey, 2011; Nozaki et al., 2013).

One or more of the characteristics of VMS deposits, like ore content, wall rocks and geotectonic environment of formation, have been used to classify them (Sawkins, 1976; Solomon, 1976; Klau and Large, 1980; Franklin et al., 1981; Lydon, 1984; Franklin et al., 2005; Piercey, 2011). Different to the above classification criteria, the VMS have been assessed in terms of relationships of main mineralization type and distinguishing characteristics, mineralization structure-texture relationship, salinity of hydrothermal fluids and oxic-anoxic conditions of formation (Scott, 1992; Galley et al., 1995; Herzig and Hannington, 1995; Goodfellow and Peter, 1996; Doyle and Allen, 2003; Goodfellow and McCutcheon, 2003; Goodfellow et al., 2003; Solomon et al. (2004a,b); Tornos, 2006; Tornos et al., 2008). Ore-forming processes and the geometric characteristics of deposits are generally controlled by the physical and/or chemical nature of the host rocks, temperature, and composition of hydrothermal fluids and properties related to the redox state of the depositional environment (Tornos et al., 2015).

* Corresponding author.
E-mail address: kurtulus.gunay@mta.gov.tr (K. Günay).

https://doi.org/10.1016/j.oregeorev.2018.08.010
Received 6 October 2017; Received in revised form 31 July 2018; Accepted 8 August 2018
Available online 11 August 2018
0169-1368/

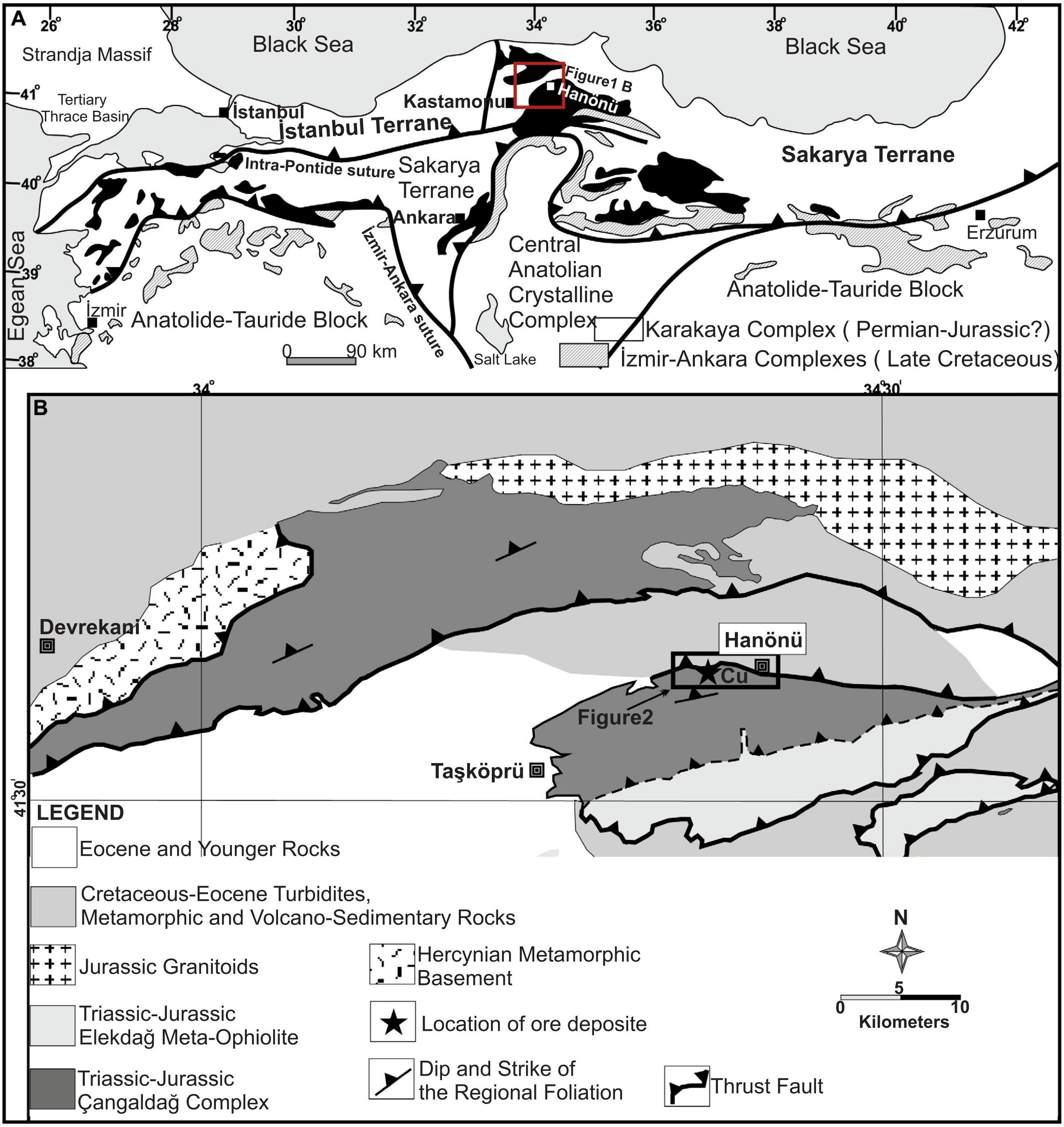

Fig. 1. Simplified regional geological map of the Çangaldağ Complex (compiled from Okay and Tüysüz, 1999; Uğuz et al., 2002; Okay et al. 2006; Göncüoğlu, 2010).

Hanönü sediment-hosted massive sulfide deposit is the first sediment-hosted massive sulfide deposit discovered in Anatolia (Turkey). Over 150 thousand meters of drilling have been completed within the area and nearly 30 million tonnes (Mt) of copper reserve have been identified by two separate study groups in adjoining areas. This is a combination of the 24.5 Mt (1.6% Cu) Cu reserve announced by Acacia Mining Company and the 4.7 Mt (0.78% Cu) Cu reserve identified in the continuation of this mineralized area by General Directorate of Mineral Research and Exploration (MTA). The aim of this article is to define the geologic, mineralogic and geochemical characteristics of the newly-discovered Hanönü massive sulfide (HMS) deposit, interpret the VMS ore genesis of Hanönü and contribute to genetic models, in addition to providing effective data for mineral exploration programs in Anatolia.

2. Regional geology

Tectonic Units forming Anatolia are generally located between large continental plates carrying Laurasia to the north and Gondwana to the south. Many continental crustal fragments rifted from these large continental plates and collided with other continental and oceanic crustal fragments to form the current Anatolian geography by the end of the Mesozoic (Yılmaz and Şengör, 1985; Göncüoğlu et al., 1997; Okay and Göncüoğlu, 2004; Göncüoğlu, 2010). Anatolia may be separated into three different tectonic units including the Pontides in the north, the Arabian platform in the south and the Anatolide-Tauride platform between the two (Ketin, 1966; Okay and Tüysüz, 1999). These tectonic units were initially separated by the Tethys oceans but were amalgamated along tectonic zones by the closure of these oceans (Fig. 1A). In

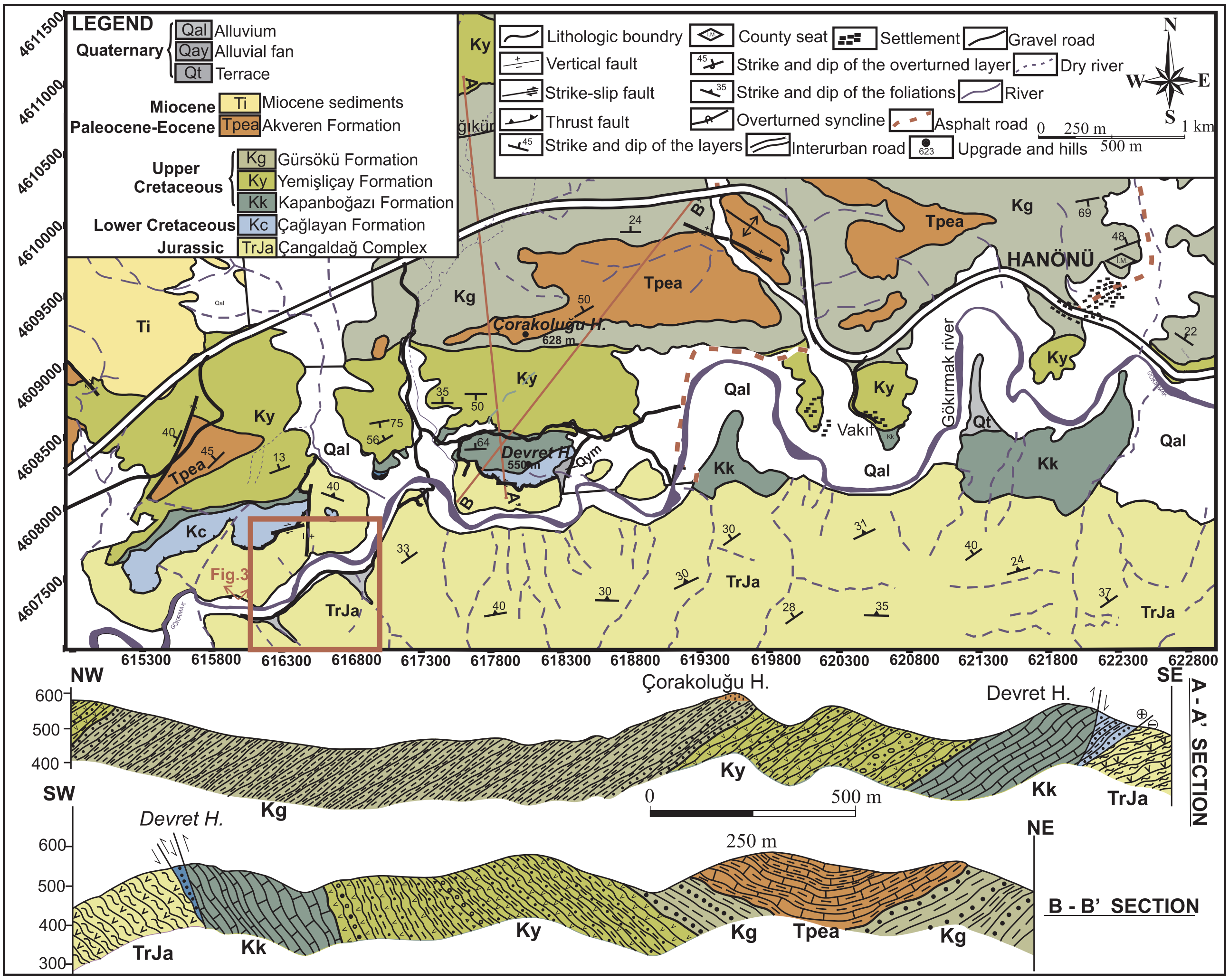

Fig. 2. Geologic map of lithologic units related to the Hanönü massive sulfide deposit.

northern Anatolia initially three terranes (Istranca, İstanbul and Sakarya) were combined during the middle Cretaceous to form the unit called the "Pontides". This Pontide unit was affected by Alpine orogenesis, and preserves the effects of the Variscan and Cimmerian orogenies (Göncüoğlu, 2010). The Anatolide-Tauride unit was severely deformed and metamorphosed during the Alpine orogeny. Based on the type and age of this metamorphism, the Anatolide-Taurides is separated into several sub-sections. The Central Anatolian Crystalline Complex comprises the largest area of Upper Cretaceous-aged metamorphic and plutonic rocks. Considering internal characteristics it is impossible to say whether this complex should be assessed as a part of the Anatolide-Tauride unit or as a separate microcontinent. The Istanbul terrane contains a Cadomian basement, with two Variscan units and a common Alpine cover. This assemblage remained joined to the Moesian platform until the Early Eocene and gained its current location with the opening of the western Black Sea (Göncüoğlu, 2010). The Sakarya terrane has a pre-Alpine basement forming a "composite unit" including tectonic assemblages with different geologic histories (Göncüoğlu et al., 1997). Tectonic assemblages forming the Sakarya composite unit include Variscan-age metamorphic units and the Karakaya complex belonging to the Cimmerian and oceanic crustal fragments belonging to Paleotethys. The common cover of these units begins in the Early Jurassic, and continues without interruption with Jurassic-early Cretaceous platform sediments. Above this, late Cretaceous flysch type sediments occur above slope facies sediments and then ophiolitic material derived from the Intra – Pontide Ocean (Göncüoğlu, 2010). The Karakaya complex is a unit with a controversial geological evolution. This complex located within the Sakarya terrane is interpreted as a Triassic-age rift (Bingöl et al., 1975), Paleozoic-Mesozoic-aged accretionary prism (Tekeli, 1981), a marginal basin opened within the Sakarya continent (Şengör and Yılmaz 1981), a Permo-Triassic-aged intraoceanic fore-arc melange and a basin on the Sakarya continent with a subduction melange from the Paleotethys (Göncüoğlu et al., 2000). This complex is divided into subunits of metamafic rocks, oceanic sediments, Hawaii-type ocean island volcanoes and their platform-slope sediments, Paleozoic-aged flysch sediments, and fragmented ophiolites (Okay and Göncüoğlu, 2004). Evaluated within the Karakaya complex, units like Çangaldağ, Elekdağ, and Domuzdağ (Fig. 1B) are proposed to be fragments related to Paleotethyan oceanic lithosphere (Okay and Tüysüz, 1999; Ustaömer and Robertson, 1999). Paleotethys ophiolites (Elekdağ, Küre), ophiolitic melange (Domuzdağ Melange) and related units [Çangaldağ metamorphic complex: Çangaldağ ensimatic island arc and related sediments (metasedimentary units containing Hanönü copper deposit)] are considered to be basin complexes which were located along the southern edge of Eurasia before the Late Jurassic (Ustaömer and Robertson, 1997, 1999; Robertson, 2002) (Fig. 2).

Studies in the recent years based on radiometric ages obtained from metavolcanics in the Çangaldağ Metamorphic complex (CMC) (Okay et al., 2014; Çimen et al., 2016, 2017) and detailed field geologic mapping suggest that, contrary to what was considered, the Çangaldağ complex and related units are not a unit belonging to the Paleotethys oceanic basins, but to a Neotethys oceanic basin (Göncüoğlu et al.,

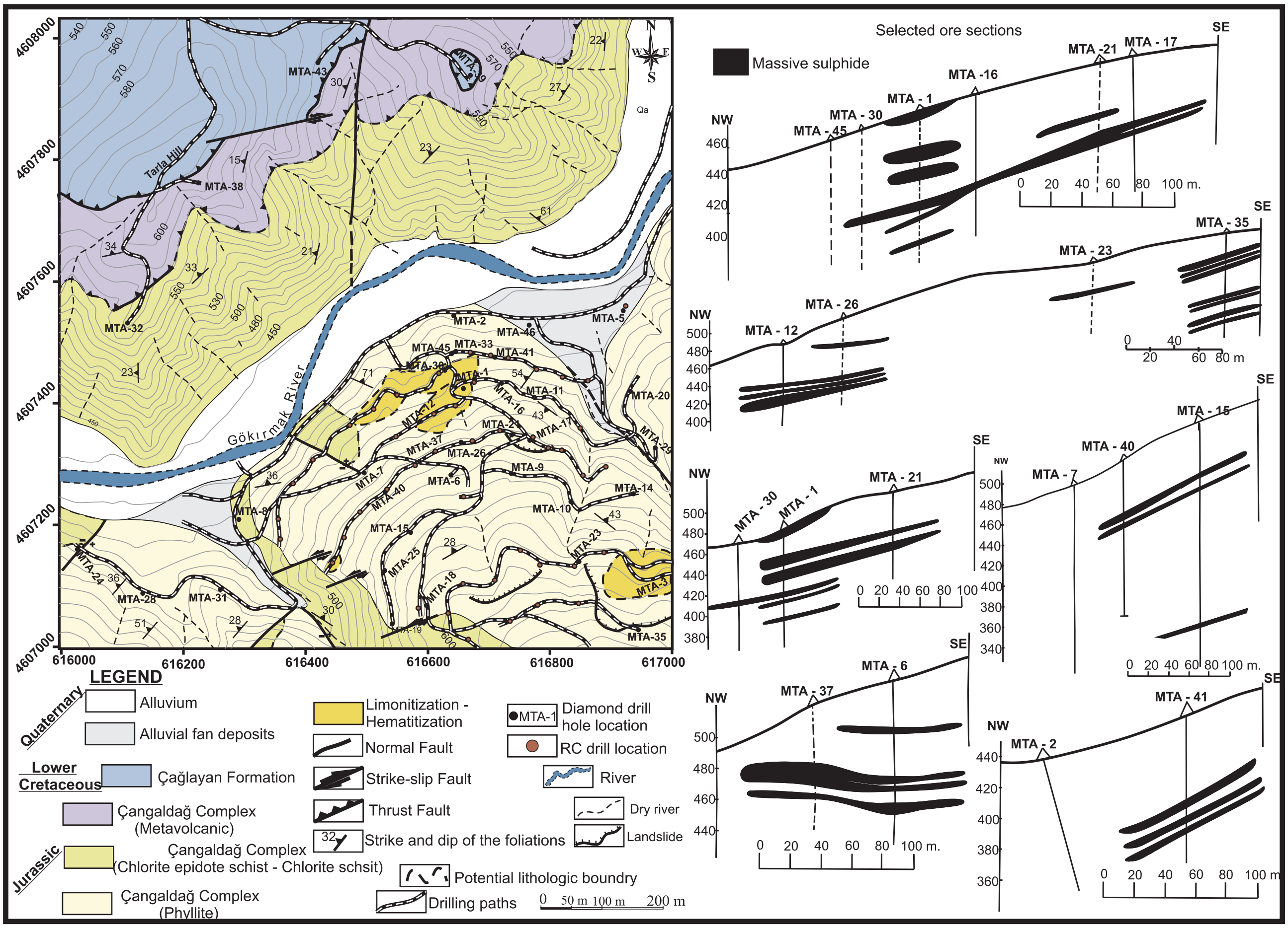

Fig. 3. Geologic map of the Hanönü massive sulfide deposit.

2008, 2012, 2014; Çimen et al., 2016). These units considered as a tectonic nappe related to the Intra-pontide suture zone give weight to the consideration that they belong to the Intra-pontide oceanic basin between the Sakarya composite terrane and Istanbul terrane. With very little data about the Intra-pontide branch of Neotethys, it is proposed to have existed in the interval from the middle Triassic to upper Paleocene (Robertson and Ustaömer, 2004; Göncüoğlu et al., 2008; Akbayram et al., 2012; Catanzariti et al., 2013).

The CMC has NE-SW orientation with nearly 45 km length and 10–15 km width and is separated into two slices by a fold-thrust belt. These slices contain ensimatic island arc volcanic units (basaltic andesites, dacite, rhyodacite, and rhyolite) and old oceanic crustal fragments (sheeted dikes, pillow basalts, and radiolarite), volcanoclastics (quartz-chlorite-epidote schist, chlorite-epidote schist, etc., phyllites) and organic-rich argillic black-colored mica schists with tectonic contacts. The whole of this allochthonous sequence contains disrupted primary relationships. The geochemical characteristics of volcanic-subvolcanic rocks within the CMC show they were produced from a subduction-modified mantle source with both arc and back-arc affinity (Ustaömer and Robertson, 1997, 1999; Çimen et al., 2016).

3. Geology of the Hanönü massive sulfide (HMS) deposit

The HMS mineralization is located southwest of the Hanönü settlement area. Mineralization is mainly found in blackish-grey phyllite dominantly found in southern sections of the Gökırmak River and a lower amount in grey-green color schists (Fig. 3, Fig. 4a-b). Phyllites (possibly black-grey shale protolith), schists (possibly siltstone/greywacke protolith) and metabasalts are units of the Çangaldağ complex. These units with tectonic boundaries were affected by deformation generally in the form of isoclinal folds and imbricates. Phyllites have well-developed foliation and are fine-grained, with iridescent luster due to mica minerals (Fig. 4b). Schists have good foliation, with slightly more solid structure and slightly larger grains compared to phyllites (Fig. 4c). Metabasalts contain minerals with green color tones due to chlorite, epidote and actinolite, occasional folding and schistose texture, while as foliation has not developed well in lower zones, massive sections are observed as interlayers (Fig. 4d). These units related to the Hanönü massive sulfide (HMS) mineralization have dominant foliation dip of 20°–70° to the northwest. Meta-sedimentary units generally show the conformable transition in drill core. Additionally, there appear to be occasional shear zones at transitions between large-grained and fine-grained rock groups and between metasediments and metamafic rocks. The upper and lower zones of massive ore, especially, are accompanied by argillic crush zones, with mylonitic-cataclastic textures (Fig. 4e–h). Tectonic and metamorphic processes have affected all units including the mineralization. Many previous studies have revealed that the area where the HMS is located is part of a large thrust-fold belt (Ustaömer and Robertson, 1999; Okay et al., 2006, 2013). All of the structural conditions and metamorphic events are related to evolution undergone by all allochthonous units to reach their current locations.

Common weathering effects observed in ore and wall rocks are limonitization and hematization. The most widespread alteration minerals observed in wall rocks are chlorite, epidote, quartz, magnetite, hematite, and gypsum. Supergene alteration products accompanying limonitization are azurite and malachite. These alteration products are located on schistosity planes in wall rocks or appear within fractures-cracks in mineralization clusters in zones close to mineralization. X-ray

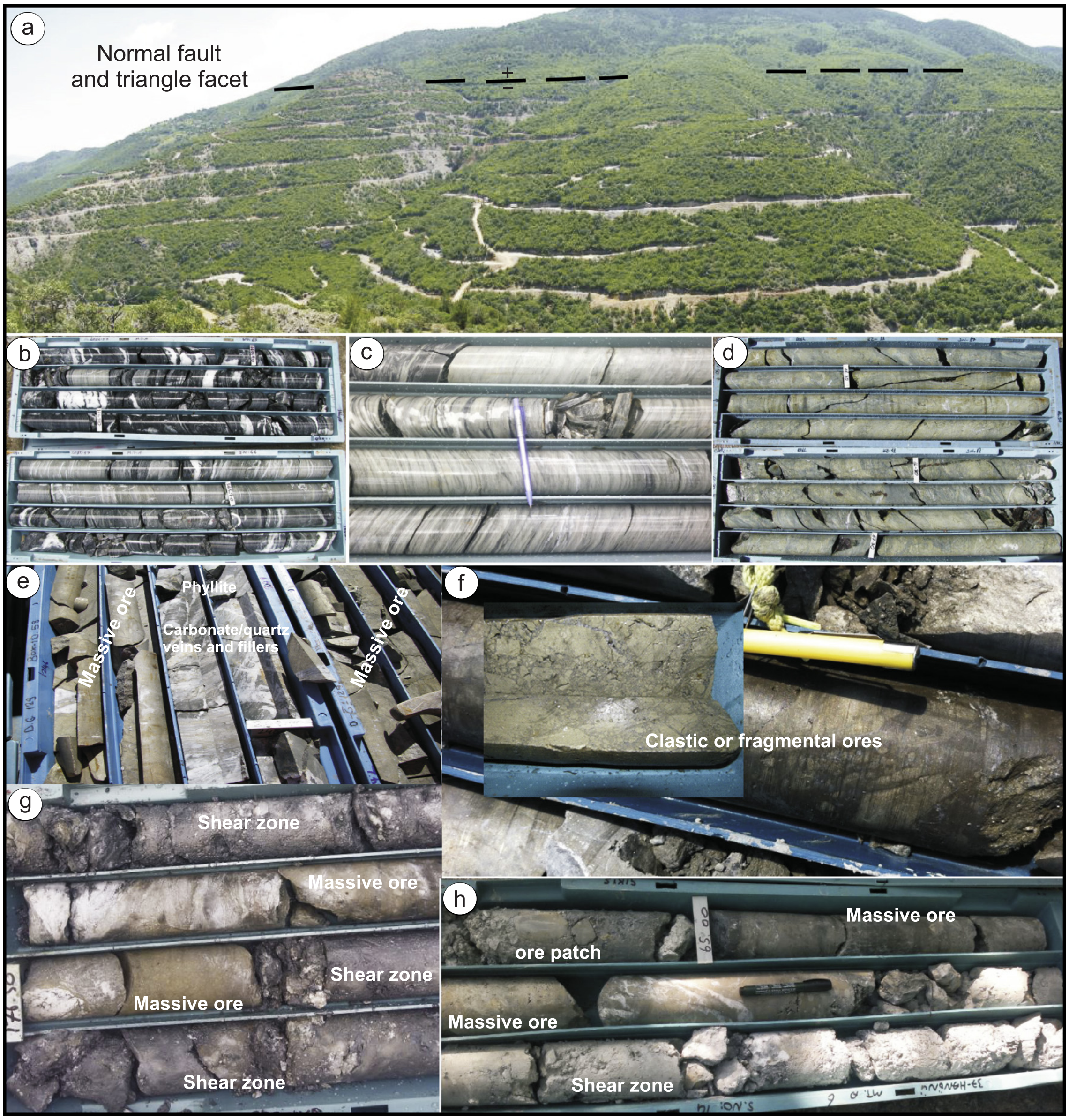

Fig. 4. a- Photograph of Hanönü massive sulfide mineralization, b- intercalations of black shale/slate phyllites with gray siltstones, c- well-developed lamination in chlorite schists and mica schists, d- chlorite-epidote-actinolite schist with the mafic volcanic source, e/h HMS ores and related clay-like crush zones with mylonitic-cataclastic texture.

diffraction analysis of crush zones related to mineralization has shown they contain chlorite, muscovite, quartz, pyrite, chalcopyrite, magnetite, hematite, ankerite and gypsum minerals. In the study area, limonitization and hematization are the most significant lithologic marker for mineralization findings. In the area of the HMS mineralization, the thickest massive sulfide zone is 20.65 m. Additionally, during exploration drilling, the highest thickness of the massive sulfide zone interlayered with wall rocks was identified as 36.70 m. The deepest drilling in the mineralized area is 1200 m. Reserve drilling found massive sulfide levels in the interval 22.50–531.20 m. The HMS mineralization is related in origin to volcanoclastics and interlayered mafic sills or lava. The lower and upper stratigraphic locations of mineralization have contact with mica schist/chlorite schist, mica schist, and mica schist/metabasics. The rocks at these contacts and some crush zones are slightly less enriched in terms of Cu and Zn content compared to others.

The HMS mineralization occurs as massive, banded and disseminated sulfides, which are the most common ore structures. The ore zone occurs within light gray color fine-grained siltstones and black shale/slates. These clastic rocks contain basaltic sills or lava layers. Meta-siltstone/greywacke and metabasalts in this metamorphosed sequence have a locally silicified, chlorite-rich matrix. In sections where the metamorphic effects are observed in meta-siltstone/greywacke, it may be described as a chlorite-epidote schist with granoblastic texture (Fig. 5a–d). Phyllites composed of black-gray color, very fine-grained shale/slate have lepidogranoblastic (quartz + sericite) textures and toward the lower zones, lepidoblastic-lepidogranoblastic textures may be described as quartz-mica schist (quartz + calcite + mica + chlorite (Fig. 5e–f). The main component of phyllites is sericite flakes less than 0.1 mm in size. These sericite flakes contain very fine-grained feldspar and quartz grains in addition to graphite levels. Metabasalts (epidote + chlorite + actinolite + albite + sphene + calcite + quartz) have disseminated pyrite content, with locally silicified sections and these rocks comprise chlorite-epidote-actinolite schists based on petrographic properties (Fig. 5g–h). X-ray diffraction (XRD) analysis of shear zones related to mineralization identified the mineral paragenesis of these zones as chlorite, muscovite, quartz, pyrite and chalcopyrite.

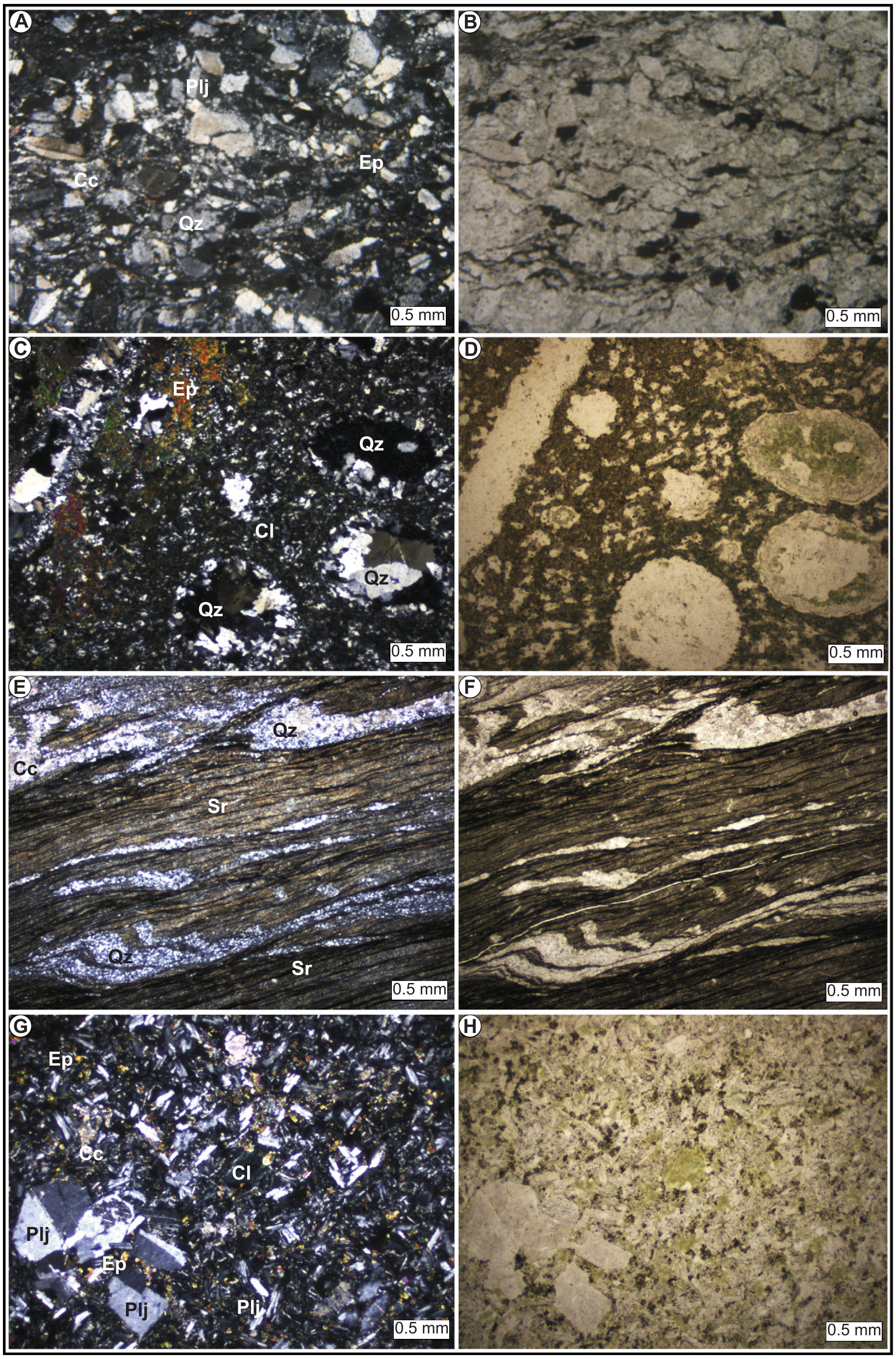

Fig. 5. Photomicrographs in transmitted crossed polarized light & plane polarized light microphotographs of HMS ore body hangingwall and footwall rocks. Volcanoclastic rock A-D, metasiltstone/metagreywacke, E-F black shale/phyllite, G-H footwall metabasalt rock (Qz-quartz, Ep-epidote, Sr- sericite, Plj-plagioclase, Cl- chlorite, Cc-calcite, A-C-E-G cross Nicol, B-D-F-H single Nicol).

Additionally, in local areas with alteration observed as lithological cap the minerals comprises hematite, magnetite, ankerite, pyrite, and gypsum.

Ore minerals comprise major pyrite, chalcopyrite, minor sphalerite and trace magnetite. Pyrites (generally 10–600 µm grain size) with massive, disseminated bands and massive bands form three different types as euhedral, anhedral and framboidal-like (Fig. 6a–c). Framboidal and anhedral pyrite grains are generally overprinted by chalcopyrite. Chalcopyrite is emplaced within fractures in pyrites and forms a second crystallization phase wrapping (post-dating) pyrites. Sphalerite is found associated with chalcopyrite. Occasional chalcopyrite inclusions are encountered within sphalerite minerals. Pyrite-chalcopyrite aggregates and quartz gangue matrix are occasionally cut by chalcopyrite-sphalerite curved-capillary-like veins. The whole sulfide mineralization system is cut by carbonate/silica veins probably developing during processes after ore formation. Additionally, completely argillized fragments, probably of hangingwall rocks, are occasionally found within the massive ore. Magnetite is in the form of independent euhedral-subhedral crystals or along the rims of chalcopyrite and sphalerite minerals (Fig. 6d). These types of magnetite crystals are observed especially in chlorite schist-phyllite rocks and follow schistosity planes. Rutile minerals observed on polished sections have anhedral form and

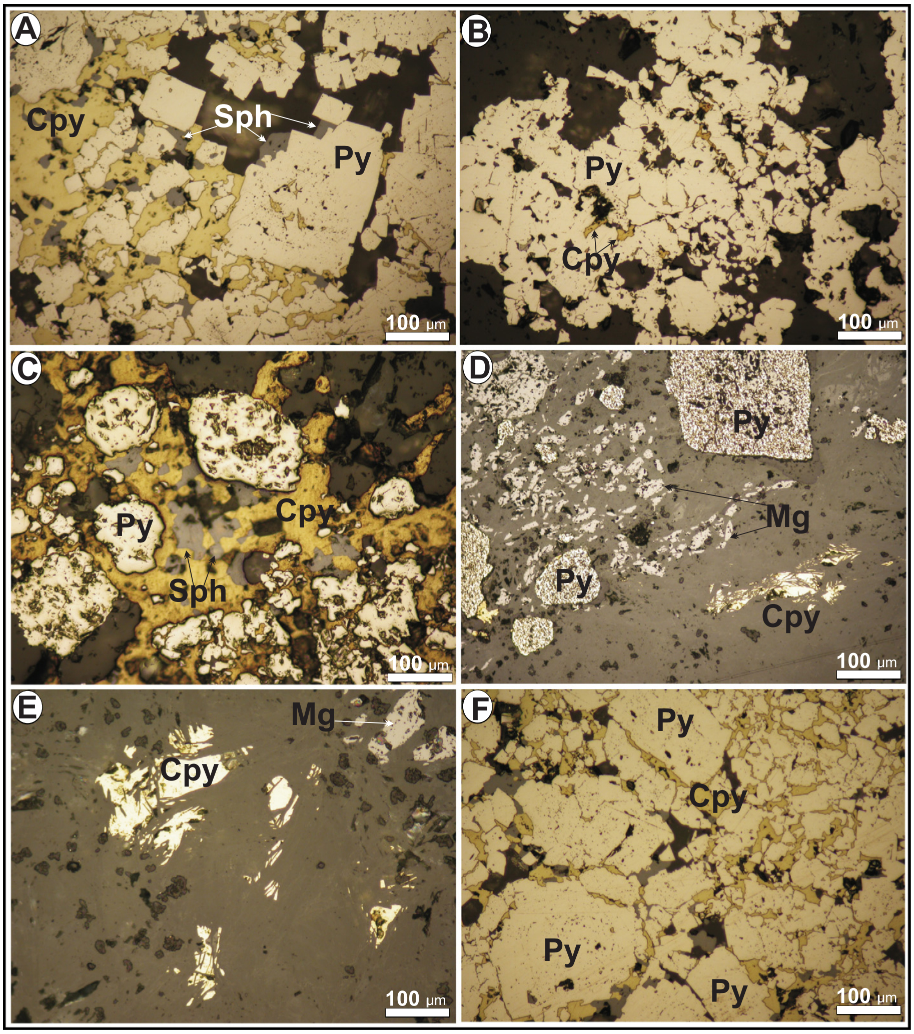

Fig. 6. Photomicrographs in reflected light showing HMS orebody; Py: pyrite, Cpy: chalcopyrite, Mg: magnetite, Sph: sphalerite (see text for details).

are occasionally altered to leucoxene. Throughout the mineralization system, deformation effects like brecciation and fracturing are observed (Fig. 6d–f).

4. Analytical methods

During discovery and reserve identification stages for the HMS mineralization, over three thousand bulk rock samples were taken from ore zones and mineralized wall rocks and analyzed in MTA (General Directorate of Mineral Research and Exploration) laboratories. The most characteristic samples were chosen from the data set and are presented as a table in the article.

For the geochemical analysis of samples, preparation methods appropriate to the character of the sample were used and analyses were completed employing XRF, ICP-OES and ICP-MS devices. After samples were dried for nearly 12 h at 60 °C, they were ground so 85% of grains were below 75 μm. For XRF analyses, samples were dried in a 105 °C oven for 4 h. Later, samples were pressed into pellet form by grinding 3 g samples with 0.9 g wax (used as binder) at 235 rpm for 15 min. The homogeneous mixture obtained was compressed into pellet form with 400 kN pressure. The prepared samples were analyzed with a Thermo ARL Advant model WD-XRF spectrometer. Analyses used the UniQuant semi-quantitative analysis method. Samples were confirmed with appropriate structure SRMs (JA-1, JA-2, JA-3, G1, JR2, 267, SI-3, NCS DC 73303). For rare earth element (REE) and trace element analyses, the triple acid solution method was used. For this method, the sample is prepared with concentration (1:2:2) ($HClO_4$ + HCl + HNO_3) + 80–90 °C water bath (2 h) + distilled water or aqua regia solution (3:1) concentration (HCl + HNO_3) + 80–90 °C water bath (2 h) + distilled water and measurements performed with ICP-MS. Using the same sample preparation method, trace elements (As, B, Ba, Be, Bi, Cd, Co, Cr, Cu, Li, Mn, Mo, Ni, Pb, Sb, Se, Sn, Sr, Ti, V, Zn) were measured with ICP-OES and Ag element analysis was performed with AAS. For Au element analysis, the sample was prepared with aqua regia ratio (1:3) (HNO_3 + HCl) + 300 °C hot plate or cupellation (fire assay + grav.) method and analysis were completed with ICP-MS.

Sulfide samples prepared for the sulfur isotope analyses were either clean pyrite crystals separated under Stereo-microscope from crushed bulk or from chalcopyrite-rich ore samples from which polished sections were prepared. Chalcopyrites were marked under the ore microscope and then about 100 mg sample in the form of powder was acquired by employing a hand-held Dremel micro-driller with a 0.5 mm silicon carbide bit to from the marked areas. Sulfide samples prepared for lead isotope analyses were bulk ore samples since the ore samples do not contain any galena. Pyrite and chalcopyrite-rich areas were marked under the ore microscope. These areas were then drilled using the micro-driller to produce about 50 mg sample for further lead isotope analyses.

Sulfur isotope analyses were carried out using the EA-IRMS (Elemental Analysis – Isotope Ratio Mass Spectrometry) (Iso-Analytical, UK). For determination of S-34, sulfide powders were converted to pure SO_2 to permit analysis with the technique. For sulfur isotope analyses,

Table 1
Results of selective geochemical analyses from the HMS ore.

Sample	Ore type	Au (ppb)	Ag (ppm)	As (ppm)	Bi (ppm)	Cd (ppm)	Co (ppm)	Cu (%)	Mn (ppm)	Mo (ppm)	Ni (ppm)	Pb (ppm)	Sb (ppm)	V (ppm)	Zn (ppm)
MTA.1-12	Massive Ore	< 40	1.8	19	< 5	< 3	200	1.8	960	10	11	42	6.0	25	760
MTA.1-20		< 40	3.3	76	< 5	8.0	230	1.0	270	18	13	71	7.0	15	2400
MTA.1-32		40	2.5	58	6.0	9.0	400	1.7	180	16	13	67	6.0	13	3500
MTA.1-37		130	3.5	77	6.0	31	310	2.75	580	11	23	110	6.0	62	10,000
MTA.6-63,70		< 40	18.1	105	< 5	13	471	3.1	1693	5.0	8.0	86	< 5	5.0	3347
MTA.6-65,00		< 40	12.2	44	< 5	< 3	201	1.0	199	< 5	11	69	< 5	< 5	2682
MTA.12-55,00		< 40	3.0	33	< 5	< 3	144	1.7	1131	16	13	23	< 5	38	1030
MTA.12-55,50		< 40	4.0	33	< 5	< 3	346	2.5	1149	17	12	27	< 5	21	1438
MTA.12-56,50		50	3.7	40	< 5	< 3	256	2.3	1759	13	10	27	< 5	20	6580
MTA.12-57,50		< 40	3.0	33	< 5	< 3	272	2.1	387	5.0	9.0	20	< 5	17	1625
MTA.12-58,50		< 40	3.3	34	< 5	< 3	287	2.3	115	< 5	9.0	27	< 5	17	2220
MTA.12-59,50		< 40	3.9	32	< 5	< 3	338	2.4	288	6.0	18	31	< 5	12	4361
MTA.12-60,50		< 40	2.8	24	< 5	< 3	152	1.3	2160	11	11	23	< 5	49	997
MTA.12-62,00		< 40	2.9	22	< 5	< 3	246	2.3	370	8.0	9.0	23	< 5	12	2657
MTA.12-63,00		< 40	4.1	15	< 5	< 3	142	3.6	1445	20	6.0	21	< 5	11	1007
MTA.12-64,00		< 40	3.7	27	< 5	< 3	162	3.5	439	10	6.0	28	< 5	< 5	1646
MTA.12-65,00		< 40	3.0	27	< 5	< 3	140	2.3	657	14	7.0	25	< 5	17	2539
MTA.12-66,00		< 40	3.0	23	< 5	< 3	112	2.0	478	13	10	23	< 5	27	2092
MTA.12-67,00		< 40	2.4	24	< 5	< 3	80	1.4	564	13	14	21	< 5	20	621
MTA.13-133		< 40	2.6	88	< 5	32	214	2.1	884	33	12	91	5.0	23	7321
MTA.13-136		< 40	2.6	88	< 5	12	238	2.3	925	16	7.0	95	7.0	19	3555
MTA.13-139		< 40	3.5	63	< 5	5	130	1.6	2980	12	23	52	< 5	49	3105
MTA.13-188		< 40	3.1	78	< 5	20	237	1.8	1761	16	22	46	< 5	12	239
MTA.13-236		< 40	1.7	62	< 5	24	141	1.0	1600	22	31	43	< 5	10	5210
MTA.21-48,95		< 40	5.1	57	< 5	6.0	293	2.3	494	< 5	9.0	126	5.0	25	1364
MTA.21-50,00		< 40	13.2	75	< 5	7.0	419	4.8	332	< 5	10	337	5.0	10	1106
MTA.21-53,00		< 40	3.3	72	< 5	6.0	302	2.6	1203	< 5	9.0	172	6.0	9.0	1295
MTA.21-54,00		< 40	3.1	54	7.0	12	347	1.7	649	7.0	12	91	8.0	11	2107
MTA.21-55,00		< 40	2.7	33	< 5	18	203	1.6	953	< 5	9.0	110	6.0	15	3320
MTA.22-386,00		< 40	1.5	84	6.0	7.0	277	1.5	1925	22	34	28	< 5	95	2550
MTA.26-27,60		< 40	3.0	63	< 5	4.0	334	2.4	439	14	10	36	< 5	47	1316
MTA.26-62,60		< 40	4.7	59	< 5	14	263	2.1	369	< 5	11	64	6.0	17	1954
MTA.26-63,50		< 40	5.5	66	< 5	10	242	2.7	380	6.0	11	58	< 5	14	1749
MTA.26-78,15		< 40	3.0	73	< 5	9	377	1.4	621	14	20	49	< 5	45	6000
MTA.26-78,50		< 40	2.5	56	< 5	7.0	291	2.1	191	9.0	12	45	4.0	19	4800
MTA.26-79,30		< 40	2.3	51	< 5	11	246	1.5	122	6.0	8.0	42	4.0	12	3170
MTA.26-79,85		< 40	2.3	13	< 5	< 3	112	2.0	748	8.0	16	16	< 5	57	795
MTA.26-80,65		< 40	1.1	50	< 5	< 3	164	1.3	486	7.0	15	28	< 5	30	587
MTA.26a-63,05		< 40	3.6	62	8.0	19	350	1.8	626	7.0	15	112	7.0	34	2081
MTA.26a-79,40		< 40	2.4	45	5.0	10	252	1.0	889	17	13	49	< 5	67	1468

(*continued on next page*)

Table 1 (*continued*)

Sample	Ore type	Au (ppb)	Ag (ppm)	As (ppm)	Bi (ppm)	Cd (ppm)	Co (ppm)	Cu (%)	Mn (ppm)	Mo (ppm)	Ni (ppm)	Pb (ppm)	Sb (ppm)	V (ppm)	Zn (ppm)
MTA.1-18	Banded Ore	40	2.4	39	< 5	7.0	160	1.05	800	13	15	49	< 5	29	2600
MTA.1-30		40	2.3	52	< 5	6.0	180	1.3	800	13	11	36	5.0	31	1600
MTA.1-31		40	5.0	59	10	< 3	510	4.5	620	17	10	67	9.0	18	2200
MTA.1-44		100	16	200	14	< 3	470	6.9	1600	13	43	150	7.0	60	2100
MTA.6-68,50		< 40	2.4	14	< 5	< 3	140	1.0	460	15	14	19	< 5	60	368
MTA.6-81,85		< 40	10.8	43	< 5	< 3	366	2.4	299	10	11	39	< 5	71	1178
MTA.12-61,70		< 40	3.7	35	< 5	< 3	162	1.7	670	10	13	21	< 5	31	1019
MTA.13-135		< 40	3.4	87	< 5	26	190	1.6	669	10	7.0	111	7.0	12	3765
MTA.13-137		< 40	2.7	57	< 5	11	128	1.0	1960	12	18	60	< 5	42	3630
MTA.13-148		< 40	3.1	72	< 5	< 3	126	1.85	> 3000	6.0	27	73	< 5	54	259
MTA.16-49,00		50	2.3	61	50	5.0	247	1.0	2316	33	26	10	< 5	144	2576
MTA.21-51,00		< 40	4.5	25	< 5	7.0	205	1.4	537	14	20	63	< 5	142	1379
MTA.21-52,20		< 40	3.4	42	< 5	33	353	3.1	640	< 5	12	138	< 5	16	5400
MTA.26-29,60		< 40	4.6	71	< 5	8.0	242	3.2	147	5.0	8.0	67	6.0	13	1260
MTA.26-30,60		< 40	2.5	37	< 5	8.0	198	1.4	497	13	15	36	< 5	50	1307
MTA.26a-61,25		< 40	2.1	81	11	18	391	1.0	1581	16	21	66	< 5	138	4420

IA-R026 (silver sulfide, $\delta^{34}S_{V\text{-}CDT} = +3.96‰$) was used for calibration and correction of the ^{18}O contribution to the SO^+ ion beam (IA-R026 is in-house standard calibrated and traceable to IAEA-S-1 (silver sulfide, $\delta^{34}S_{V\text{-}CDT} = -0.3‰$), which is an inter-laboratory comparison standard distributed by the International Atomic Energy Agency (IAEA) with internationally accepted $\delta^{34}S$ values.

Lead isotope analyses were performed with A TIMS (Thermal Ionization Mass Spectrometry) (Geochron Lab, USA), which is a magnetic sector mass spectrometer that is capable of making very precise measurements of isotope ratios of elements that can be ionized thermally, usually by passing a current through a thin metal ribbon or ribbons under vacuum. The ions created on the ribbon(s) are accelerated across an electrical potential gradient (up to 10 KV) and focused into a beam via a series of slits and electrostatically charged plates. This ion beam then passes through a magnetic field and the original ion beam is dispersed into separate beams on the basis of their mass to charge ratio. These mass-resolved beams are then directed into collectors where the ion beam is converted into voltage. Comparison of voltages corresponding to individual ion beams yield precise isotope ratios. Measured ratios corrected for mass fractionation of 0.12 ± 0.03%/a.m.u. based on replicate analyses of NBS-981; precision of ratios is better than 0.1%.

5. Geochemistry

5.1. Ore geochemistry

HMS ores form two main types: massive and disseminated-banded. Massive ore (> 40% sulfide content) comprises uninterrupted ore masses of 0.5–20.65 m thickness, while banded ore comprises ore with 0.2–10 cm thickness intercalated with hangingwall rocks. However, this distinction does not extend to a significant difference in terms of geochemical characteristics in ore structures. HMS mineralization is dominantly Cu (0.2–6.9%) accompanied by Zn (239–10000 ppm) (Table 1). Mineralization does not have economic importance in terms of other base metals. According to Cu, Zn and Pb content, the two-way correlations with other elements shown in Table 1 do not have any significant positive or negative values. However, though very weak, there is a positive correlation between Cu-Ag/As-Pb-Ag. The Au content of the mineralization is very low (< 40–130 ppb), while there is Ag of 1.1–18.1 ppm, Co of 80–419 ppm, Ni of 6–43 ppm and Pb of 21–337 ppm.

5.2. Host-rock geochemistry (hanging wall and footwall rocks)

Clastic rocks within HMS mineralization (hangingwall rocks) can be described in three different groups as black shale/slate protoliths phyllites (Table 2 – samples coded S), siltstone/greywacke protoliths chlorite schists (Table 2 – samples coded Y) and mixed schist with 5–10 cm thickness phyllite/chlorite schist intercalations (Table 2 – samples coded K). Footwall rocks are formed by metamorphosed basaltic sills or lava (Table 3 – samples coded B, chlorite-epidote-actinolite schist). Samples taken from these rock groups for geochemical analysis were assessed with LOI free elements to choose sections less affected by alteration and metamorphism for petrographic studies.

Clastic rocks display a negative correlation of TiO_2 and FeO_t against SiO_2. Additionally, while there is a clear negative correlation of major oxides like Al_2O_3, MgO, and K_2O against SiO_2 in phyllites, a strong positive correlation is observed between Al_2O_3 and TiO_2 (r = 0,92). Phyllites are slightly enriched in Mn and Al_2O_3 content (Mn > 3000 ppm; Al_2O_3 = 17–24%) and have slightly lower values for CaO, MgO, Na_2O, TiO_2, and Fe_2O_3 compared to other clastic rocks. On chondrite-normalized REE spider diagrams, clastic rocks appear to have negative Eu trend (Fig. 7). On these diagrams, phyllites and mixed schists display similar distribution patterns, while chlorite schists are slightly poor in terms of LREE compared to other rock types.

Table 2
Results of geochemical analyses for hanging wall rocks of the HMS mineralization.

Sample	S1	S2	S3	S4	S5	S6	S7	S8	S9	S10	Y1	Y2	Y3	Y4	Y5
Al_2O_3	19.5	20.5	19.3	18.1	19.6	17.1	20.1	20.6	24.1	21.4	17.7	18	15.6	17	15.9
BaO	0.02	0.02	0.02	0.01	0.02	0.01	0.02	0.02	0.02	0.02	< 0,01	< 0,01	< 0,01	< 0,01	< 0,01
CaO	0.3	0.3	0.3	0.3	0.3	0.6	0.4	0.9	0.3	0.7	0.4	0.5	3.6	2.1	4.8
Cr_2O_3	0.02	0.02	0.02	0.03	0.02	0.02	0.03	0.02	0.02	0.02	0.03	0.02	0.03	0.03	0.03
CuO	< 0,01	< 0,01	< 0,01	< 0,01	< 0,01	< 0,01	< 0,01	0.02	0.01	< 0,01	< 0,01	< 0,01	0.02	< 0,01	< 0,01
Fe_2O_3	7.5	7.9	8.5	7.3	7.8	6.8	10.4	8.9	9.2	8.3	9.8	10.7	12.1	9.9	9.3
K_2O	3.3	3.4	2.7	2.8	3.3	2.5	3.1	3.5	4	3.5	0.4	0.1	< 0,1	0.3	0.1
MgO	1.9	2.1	3.3	2	2.1	1.8	2.3	2.4	2.3	2.1	6.4	8.2	9.5	8.6	8.2
MnO	0.1	0.1	0.2	0.1	0.1	0.1	0.2	0.3	0.2	0.1	0.2	0.2	0.2	0.2	0.1
Na_2O	1.1	1.2	1.6	1.4	2.4	2.1	1	1.1	1.6	1.6	4.5	4.3	1.5	3.3	2.4
NiO	0.01	0.01	0.01	0.01	< 0,01	< 0,01	0.01	0.01	0.01	0.01	0.01	0.01	0.02	0.02	0.02
P_2O_5	0.2	0.2	0.2	0.2	0.2	0.2	0.3	0.6	0.2	0.2	0.3	0.3	0.2	0.3	0.3
Rb_2O	0.02	0.02	0.01	0.01	0.01	0.01	0.01	0.02	0.02	0.02	< 0,01	< 0,01	< 0,01	< 0,01	< 0,01
SO_3	0.17	0.11	0.05	0.21	0.2	0.4	0.9	0.05	0.09	0.08	0.2	< 0,1	0.1	< 0,1	< 0,1
SiO_2	60.5	58.5	58.3	62.5	58.6	63.6	55.6	55.7	51.6	56.1	54.9	51.4	50.5	52.1	52.8
SrO	0.01	0.01	0.01	0.01	< 0,01	< 0,01	0.01	0.01	0.02	0.01	0.01	0.01	0.04	0.03	0.05
TiO_2	0.9	0.9	0.9	0.8	0.9	0.8	0.9	0.9	1.1	1	1.4	1.7	1.3	1.6	1.5
V_2O_5	0.03	0.03	0.04	0.03	0.03	0.03	0.04	0.04	0.05	0.04	0.04	0.05	0.05	0.04	0.04
ZnO	0.01	0.01	0.01	0.01	0.02	0.01	0.02	0.02	0.02	0.02	0.01	0.01	0.03	0.01	0.01
ZrO_2	0.03	0.03	0.03	0.03	0.03	0.03	0.03	0.03	0.03	0.03	0.03	0.04	0.02	0.03	0.03
LOI	4.4	4.8	4.65	4.3	4.2	4.1	5.15	5	5.2	4.75	3.85	4.35	5.2	4.55	4.3
Total	100.02	100.16	100.15	100.15	99.83	100.21	100.52	100.14	100.09	100	100.18	99.89	100.01	100.11	99.88
Cd	< 0.1	< 0.1	< 0.1	< 0.1	< 0.1	< 0.1	< 0.1	< 0.1	0.1	< 0.1	< 0.1	< 0.1	2.5	< 0.1	< 0.1
Ce	66.1	74.6	66.1	64.4	19.9	80.5	61.6	74.3	90.9	57.9	18.7	6.8	1.7	3	5.1
Cs	0.9	1.3	0.6	0.7	0.6	1.5	1	1.7	1	0.9	0.2	0.1	0.2	0.2	0.2
Dy	3	4	2.8	3.2	1.4	4.6	3.4	3.9	4.6	2.1	1.3	1.2	0.7	0.8	0.9
Er	1.3	1.9	1.1	1.4	0.7	2.2	1.5	1.6	2.1	0.9	0.6	0.7	0.5	0.5	0.5
Eu	0.9	1.1	1	0.9	0.4	1.2	0.9	1.1	1.2	0.7	0.4	0.2	0.1	0.2	0.2
Ga	7.4	10.2	8.6	6.6	7.7	7.1	10	10.8	11.9	8.4	10.1	13.7	5.7	8	4.9
Gd	5.4	6.3	5.3	5.6	2	7.3	5.4	6.8	7.1	4.3	2.1	1.3	0.6	0.7	1
Hf	< 0,1	< 0,1	< 0,1	< 0,1	< 0,1	< 0,1	< 0,1	< 0,1	< 0,1	< 0,1	< 0,1	< 0,1	< 0,1	< 0,1	< 0,1
Ho	0.5	0.7	0.4	0.5	0.3	0.8	0.6	0.6	0.8	0.3	0.2	0.3	0.2	0.2	0.2
La	31.8	35.6	32.6	31	9.4	37.8	28.5	32.8	43.5	27.4	8.3	2.5	0.6	1.1	1.8
Lu	< 0.1	0.1	< 0.1	0.1	< 0.1	0.2	0.1	0.1	0.2	< 0.1	< 0.1	< 0.1	< 0.1	< 0.1	< 0.1
Nd	26.9	30.4	27.7	26.5	8.9	32.6	24.2	30.2	35.2	22.7	8.6	4.2	1.2	2	3.3
Pr	7.1	7.9	7.1	6.8	2.2	8.7	6.5	7.7	9.5	6	2.1	0.9	0.2	0.4	0.7
Rb	8.7	10.8	6.9	6.2	7.9	7	9	11.5	9.7	9.5	1.4	0.5	0.3	1.1	0.3
Sc	2.7	3.7	4.3	3.4	3.5	4.2	4.1	4.2	4.9	3.4	10.9	19.8	6.8	5.6	4
Sm	4.6	5.4	4.6	4.7	1.8	6	4.4	5.6	5.8	3.8	1.7	1.1	0.4	0.6	0.8
Tb	0.6	0.7	0.5	0.6	0.3	0.8	0.6	0.8	0.8	0.4	0.2	0.2	0.1	0.1	0.1
Th	9.7	13	8.9	9.5	5.5	12.1	10	12.1	15.4	9.2	< 2	< 2	< 2	< 2	< 2
Tm	0.1	0.2	0.1	0.2	< 0.1	0.3	0.2	0.2	0.2	0.1	< 0.1	< 0.1	< 0.1	< 0.1	< 0.1
Y	14.3	22.3	12.8	15.5	8.7	23.3	17.6	18.8	21.7	9.9	6.6	8.2	5.2	5.5	5.2
Yb	0.7	1.1	0.6	0.9	0.5	1.6	0.8	0.9	1.3	0.6	0.3	0.5	0.4	0.4	0.4
As	13	12	17	16	28	28	15	25	15	11	6	13	15	11	18
Co	16	15	16	12	19	23	17	20	18	21	21	18	16	14	17
Cu	100	150	100	96	110	170	85	88	57	100	73	67	97	75	68
Mn	> 3000	> 3000	> 3000	> 3000	> 3000	> 3000	> 3000	2800	1300	2000	970	1800	1400	1400	1600
Ni	58	58	56	47	54	71	43	53	45	53	54	73	54	47	45
Pb	43	44	27	32	29	31	28	25	23	27	< 5	17	25	27	19
V	34	39	35	30	34	44	26	32	24	27	64	39	28	22	49
Zn	100	110	100	94	97	130	86	100	84	98	57	84	93	79	83

(continued on next page)

Table 2 (*continued*)

Sample	Y6	Y7	Y8	Y9	Y10	K1	K2	K3	K4	K5	K6	K7	K8	K9	K10
Al_2O_3	17.1	15.6	16.6	16.3	15.9	18.2	18.4	19.6	23.4	15	16.2	14.8	15.6	17.1	15.9
BaO	< 0,01	< 0,01	< 0,01	< 0,01	< 0,01	0.02	0.02	0.02	0.03	0.02	< 0,01	0.01	0.01	0.01	< 0,01
CaO	1.1	4.3	2.7	5.4	6.3	0.3	0.4	1.3	2.1	1.1	8.3	9.6	3.8	2.7	8.9
Cr_2O_3	0.03	< 0,01	0.03	0.03	0.03	0.01	0.02	0.03	0.03	0.02	0.05	0.02	0.02	0.05	0.05
CuO	< 0,01	< 0,01	< 0,01	0.01	0.01	< 0,01	< 0,01	< 0,01	0.01	< 0,01	0.01	< 0,01	0.01	< 0,01	0.01
Fe_2O_3	9.3	11.2	10.2	11.4	11.2	7	7.7	11.6	14.8	6.4	12	7.2	8.9	11.2	11.9
K_2O	< 0,1	< 0,1	< 0,1	0.1	< 0,1	3	2.9	2.3	3.2	2.2	1	2.1	1.9	1.2	1
MgO	8.5	7.3	7.9	10.1	8.3	2.1	2.7	4.1	3.5	2.5	3.1	2.8	4.6	4.9	3
MnO	0.1	0.2	0.2	0.3	0.2	0.1	0.1	0.2	0.3	0.1	0.7	0.4	0.4	0.2	0.8
Na_2O	4.3	3.3	4.1	2.3	2.6	1.6	2	2	1.6	1.6	3.3	1.4	1.6	2.9	3.3
NiO	0.02	< 0,01	0.01	0.02	0.02	< 0,01	< 0,01	0.02	0.02	< 0,01	0.03	0.01	0.02	0.02	0.03
P_2O_5	0.3	0.5	0.3	0.3	0.2	0.2	0.2	0.2	0.3	0.2	0.3	0.2	0.2	0.2	0.3
Rb_2O	< 0,01	< 0,01	< 0,01	< 0,01	< 0,01	0.01	0.01	0.01	0.02	0.01	< 0,01	0.01	0.01	< 0,01	< 0,01
SO_3	< 0,1	< 0,1	< 0,1	< 0,1	0.1	0.18	0.05	0.02	1.22	0.18	0.2	0.02	0.05	0.02	0.15
SiO_2	53.4	50.4	51.9	43.8	47.9	62.8	60.2	52.3	42	66.5	44	49.9	55.6	52.7	43.7
SrO	0.02	0.02	0.01	0.01	0.05	0.01	< 0,01	< 0,01	0.01	< 0,01	0.02	0.02	0.01	0.01	0.02
TiO_2	1.4	1.8	1.3	1.8	1.4	0.7	0.9	1.5	1.8	0.7	1.3	1.3	1.1	1.3	1.3
V_2O_5	0.04	0.05	0.04	0.04	0.04	0.02	0.03	0.04	0.05	0.02	0.04	0.03	0.03	0.04	0.04
ZnO	0.01	0.01	0.01	0.01	0.01	0.02	0.01	0.02	0.02	< 0,01	0.01	0.01	0.01	0.02	0.01
ZrO_2	0.03	0.03	0.03	0.03	0.02	0.02	0.03	0.03	0.03	0.03	0.03	0.03	0.02	0.03	0.03
LOI	4.15	5.25	4.65	7.95	5.6	3.75	4.25	4.65	6.3	3.4	9.3	10	6.05	5.25	9.6
Total	99.8	99.96	99.98	99.9	99.88	100.04	99.92	99.94	100.74	99.98	99.89	99.86	99.94	99.85	100.04
Cd	< 0.1	< 0.1	< 0.1	< 0.1	< 0.1	< 0.1	< 0.1	< 0.1	< 0.1	< 0.1	< 0.1	< 0.1	0.1	< 0.1	< 0.1
Ce	2.4	6.6	7.5	5.7	7.2	55.2	64	39.9	23.1	30.6	62.5	16.2	40	35	55.9
Cs	< 0.1	0.1	< 0.1	< 0.1	0.3	1	0.8	0.8	0.8	1.1	0.5	0.8	0.6	0.5	0.4
Dy	0.4	1.4	1.2	2	1.4	3.1	4	3	2.5	2.1	6.7	1.4	2.1	4.2	6.3
Er	0.2	0.9	0.6	1.1	0.8	1.3	1.5	1.5	1.3	1	3.4	0.8	1.1	2.5	3.2
Eu	0.1	0.3	0.3	0.5	0.3	1	1.3	0.9	0.6	0.6	1.9	0.5	0.6	1.1	1.8
Ga	9.2	12.2	13.3	10.7	6.7	8	8.4	13	13.5	9.3	15.7	8.5	12.5	14.9	15.1
Gd	0.4	1.3	1.5	2.1	1.7	5.5	6.9	4.6	3.3	3.3	8.8	2.1	3.7	5.1	8.1
Hf	< 0,1	< 0,1	< 0,1	< 0,1	< 0,1	< 0,1	< 0,1	< 0,1	< 0,1	< 0,1	< 0,1	< 0,1	< 0,1	< 0,1	< 0,1
Ho	< 0.1	0.3	0.2	0.4	0.3	0.5	0.6	0.5	0.4	0.3	1.2	0.3	0.3	0.8	1.1
La	0.9	2.7	2.9	2.1	2.5	24.7	30.4	18.7	10.4	14.5	28.4	7.6	19.6	15.8	25
Lu	< 0.1	< 0.1	< 0.1	0.1	< 0.1	0.1	0.1	0.1	0.1	0.1	0.3	0.1	0.1	0.3	0.3
Nd	1.4	3.8	4.5	4.9	5.3	23.7	28.7	18.8	11.5	13.4	32	7.8	17.2	18.3	27.9
Pr	0.3	0.8	1	0.9	1.1	6	7.4	4.7	2.8	3.5	7.7	1.9	4.5	4.4	6.9
Rb	0.2	0.3	< 0.2	0.5	0.4	9.5	7.6	8.3	8.4	10.5	6	10.1	8	6.1	5.9
Sc	6.2	10	15.9	21.9	4.9	3.2	5.7	8.6	9.7	4.5	21.9	7.6	8.9	14.2	22
Sm	0.4	1.1	1.1	1.6	1.3	4.7	5.8	4	2.7	2.9	7.3	1.8	3.1	4.3	6.6
Tb	< 0.1	0.2	0.2	0.3	0.2	0.6	0.8	0.6	0.4	0.4	1.2	0.3	0.4	0.7	1.1
Th	< 2	< 2	< 2	< 2	< 2	7.4	8.8	6.1	5.8	7.4	5.1	< 2	5.3	5.5	4.3
Tm	< 0.1	0.1	< 0.1	0.1	0.1	0.1	0.1	0.2	0.2	0.1	0.4	0.1	0.1	0.3	0.4
Y	2.3	8.8	7	11.6	8.2	13.8	16	14	13.6	9.6	30.3	7.5	9.8	24.7	28.8
Yb	0.1	0.6	0.5	0.9	0.5	0.8	0.8	1	1	0.7	2.3	0.7	0.7	1.9	2.3
As	19	17	25	19	19	9	5	15	15	10	17	14	12	10	19
Co	17	18	19	19	16	28	30	20	28	14	20	15	17	14	18
Cu	82	110	88	71	79	106	87	168	195	65	123	113	69	85	101
Mn	2900	> 3000	2300	2000	1800	1836	1814	> 3000	> 3000	1798	3000	2653	2020	1791	2516
Ni	56	70	70	67	53	64	81	44	74	49	81	49	48	54	42
Pb	30	35	23	21	29	10	7	20	22	8	14	20	7	6	8
V	35	45	37	40	26	99	102	115	70	32	70	26	56	44	56
Zn	100	110	110	95	100	110	88	117	153	60	98	75	47	42	57

Table 3
Results of geochemical analyses for basic rocks from Hanönü area.

Sample	B1	B2	B3	B4	B5	B6
Al_2O_3	13.4	14.0	13.0	13.5	14.1	13.5
BaO	< 0,01	< 0,01	< 0,01	< 0,01	< 0,01	< 0,01
CaO	8.0	7.9	7.9	9.7	8.0	8.6
Cr_2O_3	0.05	0.04	0.04	0.05	0.04	0.04
CuO	0.01	0.01	0.01	0.03	0.22	< 0,01
Fe_2O_3	12.7	11.9	13.2	11.3	11.6	12.0
K_2O	0.31	0.73	0.05	0.30	0.68	0.38
MgO	4.56	4.62	4.42	5.72	4.99	5.13
MnO	0.24	0.36	0.17	0.27	0.36	0.28
Na_2O	3.29	2.38	3.95	1.96	2.30	2.62
NiO	0.02	0.01	0.02	0.03	0.02	0.02
P_2O_5	< 0,1	0.25	0.17	0.29	0.27	0.25
Rb_2O	< 0,01	< 0,01	< 0,01	< 0,01	< 0,01	< 0,01
SO_3	< 0,1	0.10	< 0,1	0.12	0.10	0.09
SiO_2	51.6	50.7	52.4	48.7	50.2	50.3
SrO	0.02	0.02	0.01	0.02	0.02	0.02
TiO_2	1.48	1.37	1.52	1.62	1.41	1.52
V_2O_5	0.03	0.05	0.04	0.06	0.04	0.04
ZnO	0.01	0.01	0.02	0.01	0.05	0.01
ZrO_2	0.01	0.01	0.01	0.01	0.01	0.01
LOI	4.10	5.45	2.95	6.25	5.80	5.10
Total	99.8	99.9	99.9	100	100	99.9
Cd	< 0.1	< 0.1	< 0.1	< 0.1	< 0.1	< 0.1
Ce	13.1	18.4	8.20	12.6	14.1	17.3
Cs	0.56	0.8	0.22	0.81	0.8	0.88
Dy	3.20	3.10	4.30	3.30	3.00	3.50
Er	2.10	2.30	2.40	2.00	2.10	2.30
Eu	1.10	1.05	1.20	1.00	1.30	1.02
Gd	3.10	3.20	2.70	3.10	3.40	3.00
Hf	0.98	1.35	0.87	1.41	1.31	2.65
Ho	1.30	1.00	1.02	1.20	1.05	1.00
La	6.00	8.00	3.00	5.00	6.00	8.00
Lu	0.32	0.31	0.3	0.35	0.33	0.3
Nd	10.00	12.00	8.00	10.00	10.00	12.00
Pr	2.10	3.20	1.02	2.30	2.10	2.30
Rb	10.53	20.39	18.23	17.69	21.89	24.41
Sc	23.00	21.00	28.00	19.00	17.00	22.00
Sm	3.10	3.05	3.10	3.02	3.06	3.04
Tb	1.02	1.05	1.00	1.03	1.02	1.00
Th	1.10	1.05	0.60	1.20	1.00	1.03
Tm	0.33	0.32	0.3	0.34	0.3	0.31
Y	14.00	14.00	17.00	12.00	11.00	14.00
Yb	2.20	2.10	2.30	2.00	2.20	2.40
Nb	6.18	7.05	5.6	7.53	7.06	6.9
Ta	0.13	0.19	0.09	0.23	0.2	0.17
Sr	219	305.6	281.2	390.3	261.7	259.2
Ba	79.4	113.9	64.23	94	103.4	130.1
Zr	51.05	48.73	49.48	53.58	54.23	59.38
Cr	55.03	79.47	21.76	128.9	100.2	68.58
Pb	2.86	4.03	0.78	5.71	5.5	4.14
V	351.8	476.3	502.8	496.9	425.4	460.6

Additionally, in terms of total REE content, chlorite schists are more depleted. Trace element distribution in clastic rocks shows that phyllites and mixed schists have higher Ce (16.2–90.9 ppm) and Th (4.3–12.1 ppm) values compared to chlorite schists. Especially phyllites contain higher values for elements like Cu, Mn, As and Zn compared to other groups.

The LOI values (2.95% and 6.25%) obtained from analyses of metabasalts indicate these rocks may have been affected by hydrothermal alteration, low degree metamorphism or seafloor alteration. These types of alteration may cause mobilization of the majority of major elements and LILE elements (apart from Th) in rocks. Contrary to this, the HFSE and REE elements are mainly immobile and are not affected much by this type of alteration (Pearce and Cann, 1973; Floyd and Winchester, 1978). As a result, HFSE and REE elements were used to assess geochemical results. The major, trace and REE analysis results for metabasalt samples are given in Table 3.

As the metabasalt samples analyzed had high LOI content, the Winchester and Floyd (1977) Nb/Y – Zr/TiO_2 variation diagram (Fig. 8a) was used as it is the most useful geochemical classification for altered volcanic rocks and samples fell in the subalkaline lava series. The SiO_2 content of samples varied from 48.7 to 52.4%, while Mg# ($100 \times Mg^{+2}/(Mg^{+2} + Fe^{+2})$) varied between 50 and 60 and high Mg# values indicate that these samples partially preserve the primary magma composition. With the aim of being able to interpret the paleotectonic environment of the rocks, Ti/100-Zr-Sr/2 and Hf/3-Th-Ta variation diagrams were used. On these diagrams, the metabasalts fall within the calcalkaline and island arc tholeiites fields. This tectonic environment data indicates that the samples were derived from a source including island arc components (Fig. 8b).

With the aim of determining the composition and nature of the source area for the samples, n-type MORB-normalized multi-element spider diagrams were created (Fig. 8c–d). Whole rock samples typically display enrichment in LILE, HFSE, LREE, and MREE compared to N-MORB values and very slight depletion in HREE. Though this data is appropriate for typical OIB (or intraplate) trends, the HFSE elements such as Nb and Ta display negative anomalies relative to the adjacent LILEs and. The scattered LILE element patterns observed in a portion of the samples are most probably due to the effects of alteration, supported by the high LOI values. The samples are plotted on Sun and McDonough's (1989) chondrite-normalized REE diagram in Fig. 9d. As seen on Fig. 9d all samples display neither enrichment nor depletion for any REE elements, with samples presenting an almost linear trend from LREE to HREE (La/Yb_N = 0.9–2.7; $_N$ expresses normalized values). Though they present a trend in accordance with MORB and island arc tholeiite values, LREE displays an enrichment trend compared to MORB values.

6. Discussion

Çangaldağ Metamorphic Complex may be considered as a large block within an accretionary wedge. The lithologic members within this block display tectonic boundary relationships among themselves. In this area with chaotic relationships between lithologic units, investigation of geochemical data from the HMS mineralization area does not have the aim of explaining the Mesozoic evolution of the Central Pontides. There are significant studies at regional scale related to this topic in the literature (Okay et al., 2006, 2013, 2014; Göncüoğlu et al., 2008, 2012, 2014; Akbayram et al., 2012; Çimen et al., 2016, 2017). However, mineralogic and geochemical markers of rocks related to the HMS mineralization provide important clues to understanding the genetic characteristics of mineralization.

The HMS ores probably formed in the same paleotectonic environment or associated section as the host rocks. The regular stratigraphy with an uninterrupted sequence of volcanoclastics, the interlayering of mafic lava or sills, the mineralization of immature clastics related to mafic lava or sills and the metamorphism of the whole sequence all support the consideration that they formed together in a similar paleotectonic environment. Though these host rocks experienced low degree metamorphism, they carry useful data to identify their sources. Additionally, the chemistry of mafic lava provides important data as mentioned above compared to volcanoclastics.

6.1. Geochemical markers in mafic and clastic rocks associated with ore mineralization

OIB- (ocean island basalts) and MORB- (mid-ocean ridge basalts) type basaltic rocks display enrichment in Nb, Ta and Ti elements and depletion in Pb on multi-element spider diagrams normalized to N-type MORB or primitive mantle (Hofmann, 1986, 1988, 1997). Contrary to this information, on PM-normalized spider diagrams rocks related to HMS mineralization are relative weakly depleted in Nb and Ta and enriched in terms of Pb and this data typically does not indicate the source area for OIB or MORB. The multi-element spider diagrams in

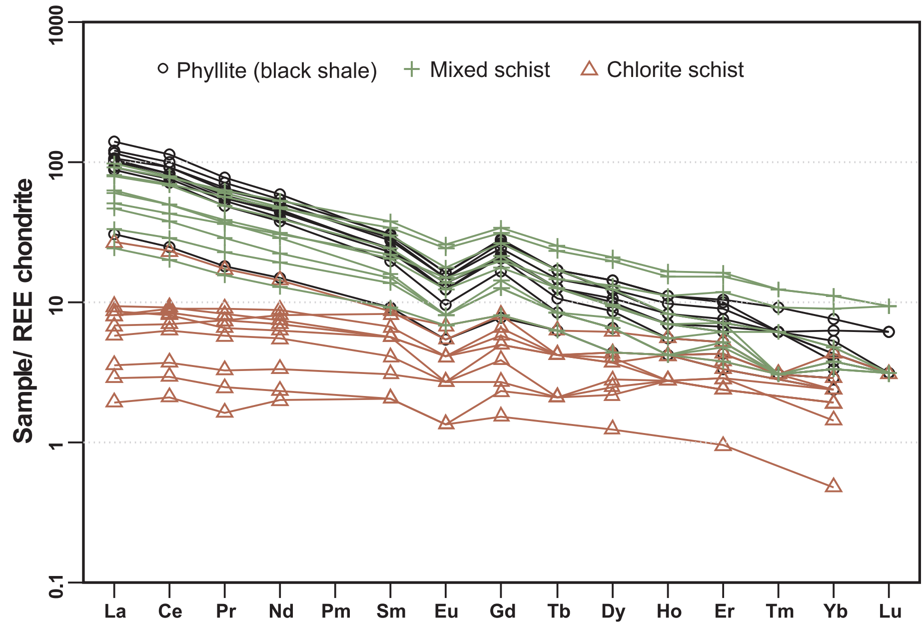

Fig. 7. Chondrite-normalized spider diagram of metasedimentary rock (Chondrite normalized value from Boynton, 1984).

Fig. 8c indicate that whole rock samples were depleted in Nb and Ta and at the same time enriched in Pb, which indicates the tectonomagmatic environment that formed these mafic rocks may have been metasomatized due to subduction.

In order to determine the nature of the mantle source region, we produced the Ta/Yb versus Th/Yb diagram. The basaltic samples related to HMS mineralization display deviations from mantle array with increasing Th/Yb ratios in Fig. 9a. This trend indicates a mantle source containing a subduction component for studied samples. To test this hypothesis, an attempt was made to observe the presence of enrichment of LILE elements compared to HFSE on LILE-HFSE element diagrams normalized to N-type MORB given in Fig. 9b. The (LILE/

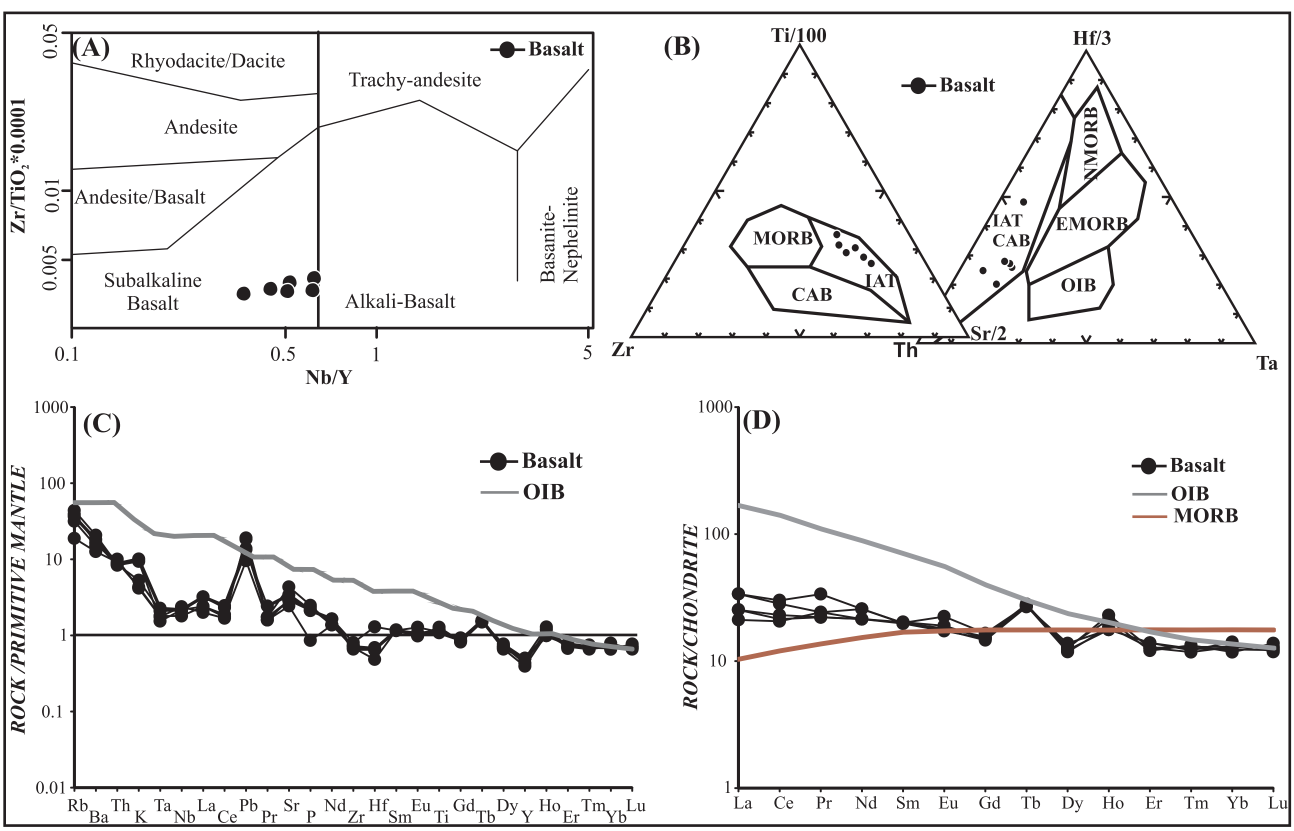

Fig. 8. A- Geochemical rock classification diagram using immobile elements (Winchester and Floyd, 1977), B- Paleotectonic environment interpretation based on immobile elements in metabasalt samples MORB-Mid Ocean Ridge Basalt; IAT-Island Arc Tholeiite; CAB-Calc-alkaline basalt; OIB-Ocean Island Basalt (Pearce and Cann, 1973; Wood, 1980). C- Multi-element spider diagrams normalized to primitive mantle values for metabasalt samples, D- REE spider diagram normalized to chondrite values (Sun and McDonough, 1989) for metabasalt samples.

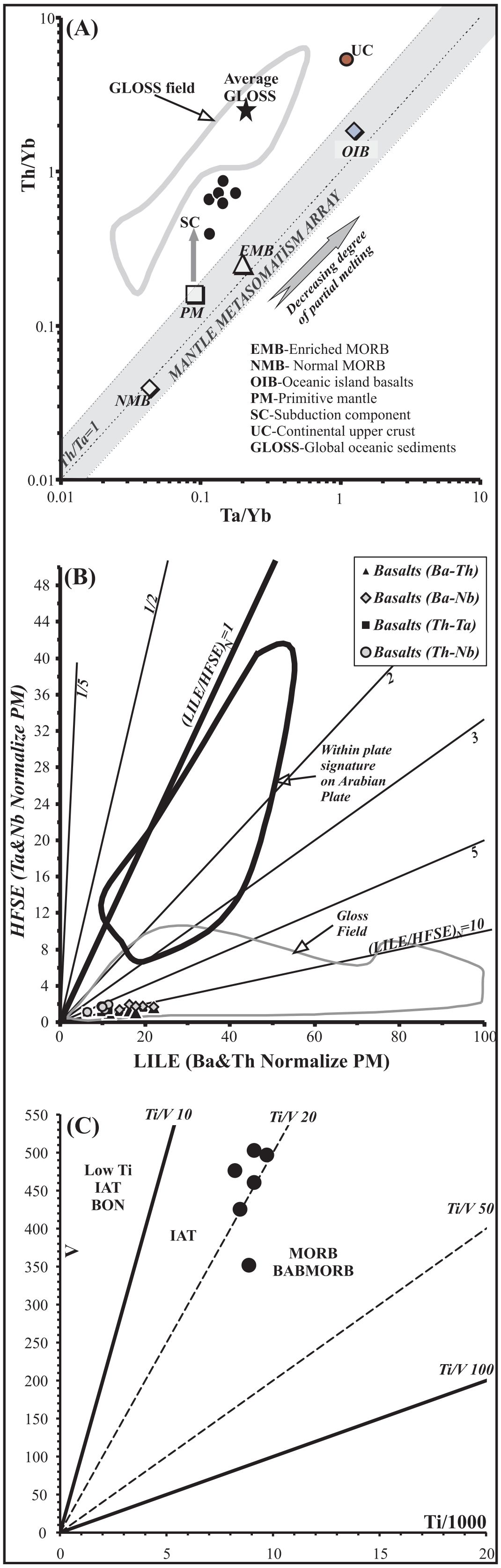

Fig. 9. A-B- Two-way discrimination diagrams prepared according to incompatible element and LILE-HFSE ratios in samples EMB, NMB, OIB, and PM are from Sun and McDonough (1989), UC is from Taylor and McLennan (1985), GLOSS is from Plank and Langmuir (1998), Field of the Arabian plate is from Lustrino and Wilson (2007), Shaw et al. (2003), and Krienitz et al. (2006). C-Ti/1000 vs. V two-way discrimination diagram (Shervais, 1982).

HFSE)$_N$ values of the samples varied between 5 and 10 and this situation indicates the mantle source region for the samples was enriched with subduction components. Additionally, it may be considered that the trends observed in Fig. 9a and b may reflect continental contamination; however the low La/Nb values of samples related to HMS mineralization indicate that they were not affected by continental contamination or that contamination was at negligible (Hart et al., 1989; Saunders et al., 1992).

Shervais (1982) stated that if the Ti/V values of basaltic samples is < 50, these samples were derived from sources enriched with subduction components and not from OIB similar sources. Samples related to HMS mineralization have low Ti/V ratios (18–22) which indicate that samples may have been derived from a source enriched in subduction components. The samples on the Ti/1000 vs. V diagram (Fig. 9c) fall in the typical island arc tholeiite area.

Determination of partial melting processes affecting the nature and area of the mantle source may reveal the partial melting processes, the source mineralogy controlling initiation and chemical basis of samples associated with HMS mineralization (Thirlwall et al., 1994; Shaw et al., 2003; Peters et al., 2008). During partial melting of a spinel peridotitic or garnet peridotitic source REE participate in different solid mineral/melting phase coefficients of the source area (Shaw et al., 2003). Enrichment of moderate rare earth elements (MREE, Am, Tb, Dy, Gd) compared to heavy rare earth elements (HREE, Yb, and Lu) only occurs in facies with garnet in the residual phase ($^{Garnet\text{-}melt}D_{Yb}$ ~ 4; $^{Garnet\text{-}melt}D_{MREE}$ ~ 0,21–1 McKenzie and O'Nions, 1991). This situation produces high MREE/HREE ratio in garnet facies partial melts and creates large differences between the melt and source ratios (Shaw et al., 2003; Wang et al., 2004; Peters et al., 2008). Contrary to this, in spinel facies partial melts there is very little variation in MREE/HREE during melt fractionation and the source ratios will be very similar to the melt ratios ($^{Spinel\text{-}melt}D_{Yb}$ ~ 0.01; $^{Spinel\text{-}melt}D_{MREE}$ ~ 0.01; $^{Clinopyroxene\text{-}melt}D_{Yb}$ ~ 0.28; $^{Clinopyroxene\text{-}melt}D_{MREE}$ ~ 0.30 McKenzie and O'Nions, 1991).

In the light of these approaches, the melt modeling created using Dy/Yb – Yb ratios for basaltic sill and lava samples related to HMS mineralization are given in Fig. 10a. This modeling study used the nonmodal batch melting equations proposed by Shaw (1970). The modeling results given in Fig. 10a show that the source area to create the sill or lava samples could not be primitive mantle alone or depleted MORB. Samples related to HMS mineralization display greater enrichment in La and Dy compared to PM and DMM sources and show characteristics that did not derive from a single source. The melt modeling curve reveals a mixture of PM and DMM sources and creating a Gr-Sp-Peridotite mantle mineralogy creates a trend compatible with the studied samples. Melts of between 8 and 15% of this type of source would create a mantle source area that can form the samples associated with HMS mineralization.

To determine the melts for back-arc basins and oceanic island arcs, the Nb-Yb melt diagram recommended by Pearce and Parkinson (1993) may be used. This diagram provides specific results related to melting of spinel peridotite-type mantle sources and enrichment and depletion areas according to fertile MORB mantle (FMM). Additionally, to compare diagrams, some island arc samples were also plotted. As seen in Fig. 10b, samples associated with HMS mineralization and lava from the Elazığ-Malatya region containing back-arc characteristics fall in the enrichment compared to FMM area. This data indicates that melt formed in a back-arc basin enriched in subduction components and were enriched compared to primary MORB mantle (compared to FMM).

Tectonic discrimination and incompatible element pair diagrams show that the samples may be island arc tholeiite species. Trends observed on spider diagrams and two-way variation diagrams show depletion in Nb and Ta elements relative to the adjacent LILE and REE elements and enrichment in Pb so samples related to HMS mineralization may have been affected by subduction components. Data obtained from partial melting modeling show that the mantle source had different ratios of both garnet and spinel and at the same time revealed

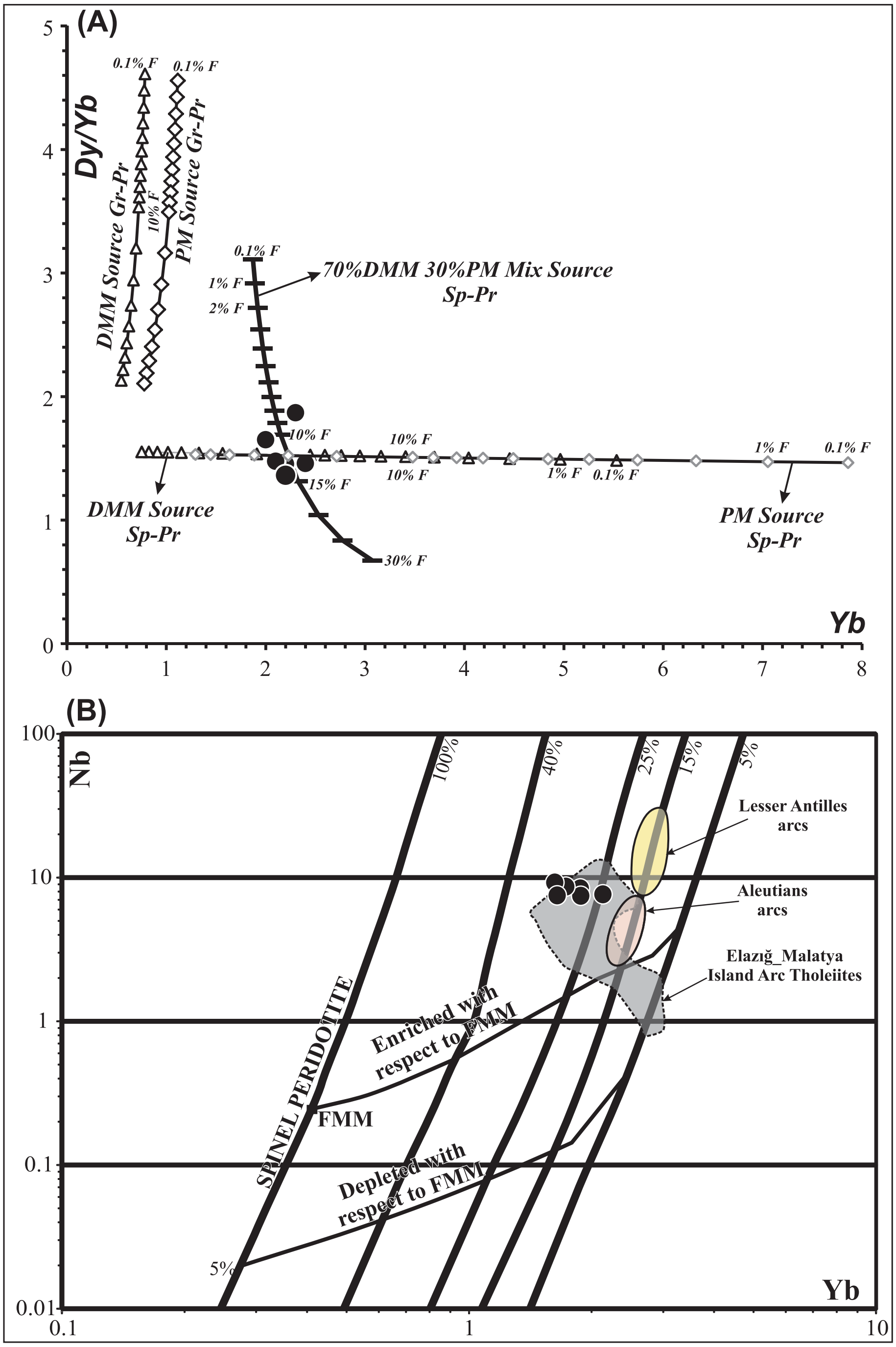

Fig. 10. A- Mantle melting model created using Dy/Yb and Yb element ratios. For the model, source mineral mode was taken from McKenzie and O'Nions (1991) with melting mineral mode taken from Thirlwall et al. (1994) (source mode for Gr-Sp-peridotite 0.55% Ol, 0.24% Opx, 0.15% Cpx, 0.04% Gr, 0.02% Sp, melting mode 0.05% Ol, 0.05% Opx, 0.28% Cpx, 0.35% Gr, 0.27% Sp). Depleted MORB (DM) values were taken from Workman and Hart (2005) and fractionation coefficients were taken from McKenzie and O'Nions (1991). B- Mantle melting model created using Yb vs. Nb element ratios (Pearce and Parkinson, 1993). With the aim of minimizing fractionation and contamination effects on this diagram, samples associated with HMS mineralization were normalized to 9% MgO values.

that mixtures of 70% back-arc depleted MORB mantle and 30% asthenospheric melts with 8–15% melting degree may have formed Hanönü basalts. If fluids derived from the previously subducted oceanic crust metasomatized lithospheric mantle, traces of subduction components may be observed in the chemistry of melt samples from this type of source. The idea that the studied samples may represent a mixture of small degree melts of asthenospheric mantle and DMM melts metasomatized by fluids from previously subducted oceanic crust may be a valid process for the source area. This process may be explained by adiabatic uplift of asthenospheric mantle and mixture of DMM type mantle enriched with subduction components in back-arc basins and high degrees of melting that may form at shallow levels.

Using the chemical components of clastic rocks, information may be accessed about the sources, basic composition and weathering processes of these rocks (Bhatia and Crook, 1986). The low degree of metamorphism experienced by clastic rocks associated with HMS ores probably affected basic geochemical composition. Additionally, the variation in elemental composition of these rocks is probably related to mineral varieties. In modern hemipelagic sediments, quartz, feldspar, mica, albite, muscovite, biotite, chlorite, illite, smectite, magnetite, zircon, titanite, and apatite minerals occur (Leybourne and Goodfellow, 1994). Highly weathered quartz grains and corroded zircons, especially, indicate a metamorphosed continental basement (Goodfellow et al., 2003). However, on thin sections of clastic rock associated with HMS ores, zircon minerals were not encountered and weathered quartz grains were not observed. Additionally, the chemical analysis results of these rocks had very low values of zircon content compared to modern hemipelagic sediments. This situation generally leads to consideration that the clastic rocks associated with HMS ores did not come from a continental basement but maybe from a very mature oceanic island

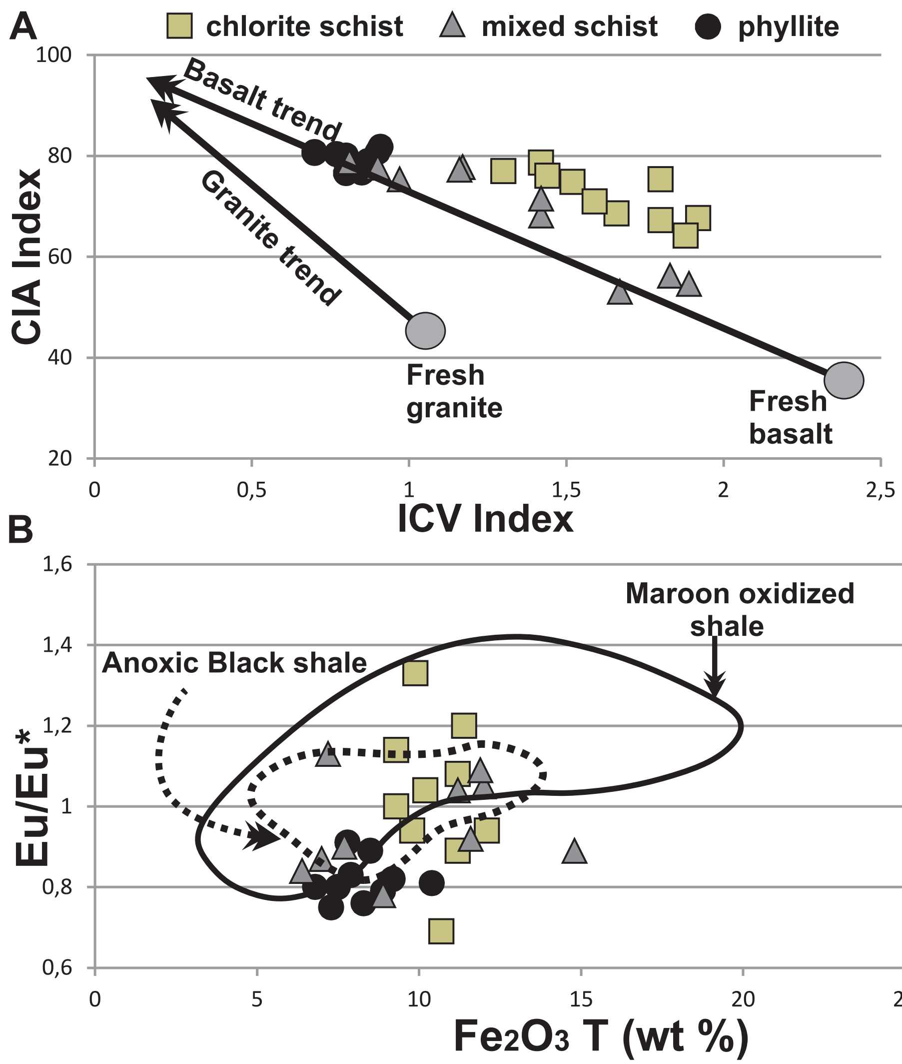

Fig. 11. Classification diagrams for clastic rocks related to HMS ores. A- Chemical Index of Alteration (CIA) and Index of Chemical Variation (ICV) in HMS ore-related clastic rocks (diagram from Lee 2002). B- Eu/Eu* vs. Fe_2O_3 (total) plot for clastic rocks from HMS deposit. Maroon oxidized shale and black shale field from Goodfellow et al., 2003. (Eu/Eu* N = EuN/ (SmN × GdN)0.5, where N = NASC normalized values).

source. The samples from interlayers of basic sills and lava within these clastic rocks reflect a back-arc rift environment, while clastic rocks support the idea of a rifting environment close to a volcanic arc with deposition fed from arc volcanics.

Rare earth element (REE) distribution in clastic rocks is clearly linked to the micaceous mineral phases. Typically, the abundance of REE elements concentrated in fine and large-grained (clay-rich) pelagic marine sediments reduces with the increase in grain size (Goodfellow and Blaise, 1988; Liu et al., 1988; Goodfellow et al., 2003). Clastic rocks related to HMS ores show enrichment in LREE on chondrite-normalized REE patterns (see, Fig. 7). On this diagram, a slight negative Eu trend and a mild depletion trend continuing from Gd to Lu is observed. Contrary to this, turbiditic sequences derived from cratons are typically enriched in LREE, have a negative Eu trend, a slight trough between Tb and Tm and flat HREE pattern (McLennan, 1989). This situation supports the idea that clastic rocks associated with HMS ores were deposited in an environment close to a volcanic arc. The chemical index of alteration (CIA) formulated by Nesbitt and Young (1982) shows the high destruction of plagioclase. CIA ($[Al_2O_3/(Al_2O_3 + CaO + K_2O + Na_2O)] \times 100$) values are lower than 50 for unweathered igneous and metamorphic rocks and 100 for pure kaolinitic remnants. The chemical index of alteration obtained values of CIA > 80 for clastic rocks related to HMS ores. Patterns on chondrite-normalized REE distribution had negative Eu anomaly, in accordance with low plagioclase content of clastic rocks associated with HMS ores. Together with the CIA index, to obtain better discrimination of rock pattern types the index of compositional variability (ICV: $CaO + K_2O + Na_2O + Fe_2O_3(t) + MgO + MnO + TiO_2)/Al_2O_3$) including is given in Fig. 12a. The average basalt and average granite fields used on the diagram in Fig. 11a are taken from Lee (2002). The CIA and ICV values for clastic rocks state that these rocks display a basaltic trend. This situation may indicate that these rocks were sourced from oceanic crust components rather than continental crust and deposited in an associated environment.

The majority of REEs are trivalent under stable conditions in the crust, while Eu is typically bivalent under reducing conditions and high temperatures (Sverjensky, 1984). Under reducing conditions, as a result of the reaction of rocks containing Ca plagioclase with hydrothermal fluids, these rocks substitute Sr with Eu due to the similar ionic radii of Eu^{+2} and Sr^{+2}. Thus, the result of the reaction between hydrothermal fluids and plagioclase produces positive Eu/ Eu^* anomalies (Michardet al., 1983; Barrett et al., 1990; Goodfellow et al., 2003). The chalcophile element iron is commonly enriched in modern anoxic sediments (Brumsack, 1989). Under anoxic conditions, pyrite formation is typical within black shales together with low MnO values (Vine and Tourtelot, 1970; Cooper et al., 1974; Brumsack, 1989). On Eu/Eu^*

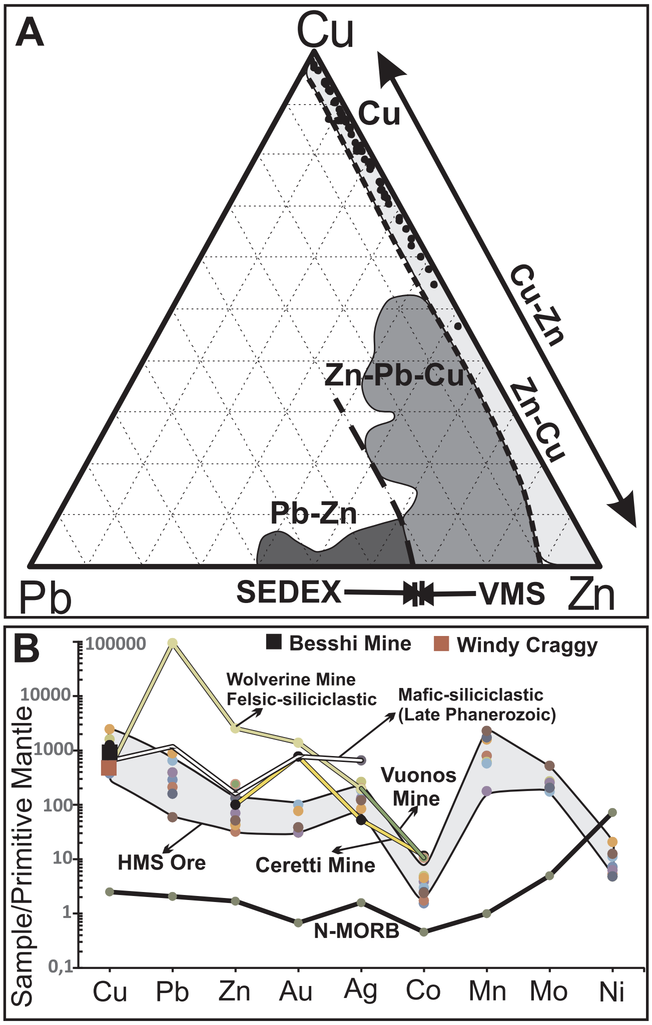

Fig. 12. A- Base metal classification scheme for VMS deposits (Franklin et al., 1981; Large, 1992). B- spider diagram showing metal ratios normalized to primitive mantle (Primitive mantle values from Hofmann, 1988; Wolf and Anders, 1980; Taylor and McLennan, 1985 and N-MORB values from Doe, 1994; Keays and Scott, 1976; Hamlyn et al., 1985). Late Phanerozoic Mafic-siliciclastic VMS values from Barrie and Hannington, 1999; Besshi (Japan) and Besshi-type deposit is Windy Craggy (British Columbia) metal values from Peter and Scott (1999) and Peltonen et al. (2007); Keretti mine and Vuonos mine (USA and Norway) metal values from Fox (1984); Wolverine mine (Canada) metal values from Bradshaw et al. (2003).

against Fe_2O_3 $_{(total)}$ diagrams for sedimentary rocks (Fig. 12B), Eu and Fe are used due to their differentiation properties linked to the behaviors described above. While anoxic black shales containing massive sulfide mineralization at Bathurst Mining Camp have Eu/Eu* values in a limited interval (0.8–1.1), the Eu/Eu* values in oxidized shales have a broad interval (up to 1.4) (Goodfellow et al., 2003). In this situation, black shale-sourced phyllites related to HMS ores display similar characteristics and reveal the anoxic nature of phyllites. The Eu/Eu* values of phyllites associated with HMS ores (0.7–0.9) are compatible with anoxic black shales and have a limited interval. Additionally, mixed schist and chlorite schist have Eu/Eu* and Fe_2O_3 $_{(total)}$ values in a broad interval (Fig. 11b).

6.2. Ore deposit classification and mineralization style

Massive sulfide deposits have been classified by many researchers considering ore composition, ore composition ratios, possible tectonic environment and dominant host-rock lithology as the principle criterium (Hutchinson, 1973; Solomon, 1976; Sawkins, 1976; Klau and Large, 1980; Franklin et al., 1981; Barrie and Hannington, 1999). Additionally, the shape of mineralization as mound-style mineralization, stratiform deposits in anoxic settings and sub-seafloor replacement have been determined as basic factors controlling massive sulfide mineralization (Tornos et al., 2015).

Classification of the VMS deposits based on base metal content (Cu-Zn-Pb) is one of the simplest and most commonly used classifications (Franklin et al., 1981, 2005; Large, 1992; Galley et al., 2007). This classification of the VMS deposits yielded three main groups as Cu-Zn, Zn-Cu, and Zn-Pb-Cu. According to Cu-Pb-Zn base metal concentration, the HMS ores are within the Cu-Zn group of the VMS deposits (Fig. 12a). The HMS mineralization is similar to mafic-siliciclastic type VMS formations (Barrie and Hannington, 1999) in terms of host-rock characteristics and Cu-rich nature. On the spider diagrams of metals normalized to the primitive mantle, HMS mineralization is depleted in Au-Ag and in terms of general Zn-Pb content compared to Late Phanerozoic mafic-siliciclastic (MS) formations. Additionally, the Cu content of the HMS mineralization and highest contained Zn-Pb values are similar to MS mineralization (Fig. 12b). Many very large VMS mineralization globally like Besshi (Japan), Windy Craggy (British Columbia), Ceretti mine (USA) and Vuonos (Norway) display MS mineralization characteristics (Barrie and Hannington, 1999; Pirajno, 2009). However, these deposits basically have similar Cu content while each has unique values for other metals. The felsic-siliciclastic type Wolverine mine (ensialic back-arc ocean basin) is Pb-Zn-Au rich which is characteristic of the tectonomagmatic environment and felsic volcanism that formed the mineralization (Bradshaw et al., 2003). This is an example of the effect of tectonomagmatic environment and associated volcanism on VMS mineralization.

Mafic-siliciclastic-type VMS deposits are generally associated with continental rifts (Pirajno, 2009; Pirajno et al., 2016). Siliciclastic rocks shaped by a high-energy environment contain angular quartz and lithic fragments within a matrix rich in sericite and clay content, and typically interlayers of basaltic lava are characteristic (Pirajno et al., 2004). Considering the lithostratigraphic types of VMS deposits, back-arc mafic or pelitic-mafic (Franklin et al, 2005; Galley et al., 2007; Pirajno et al., 2016) lithostratigraphy is compatible with Besshi-type VMS deposits (Fox, 1984). The mafic-volcanoclastic lithostratigraphy of HMS mineralization is similar to the Besshi-type VMS deposits. Contrary to this, the tectonomagmatic environment of HMS mineralization is a back-arc rift region developing on oceanic lithosphere. The HMS mineralization is an example showing that Besshi-type mineralization may develop in rifting areas on oceanic lithosphere.

The HMS ore zone has irregular geometry and distribution within volcanoclastic and black-shale sourced phyllites characterized by a chlorite-rich matrix. Structurally volcanoclastics and phyllites form the hangingwall section of the ore. The basaltic lava or sills form the footwall section associated with mineralization. This general description shows the mineralization zone varies depending on stratigraphic location. Though volcanoclastics derived from black shale and siltstone/greywacke experienced low degree metamorphism, occasionally primary textural features are preserved. Flame structures are primary structures of sedimentation due to gravitative subsidence of siltstone within immature shales (Fig. 13a–b). These types of structures probably reflect the immature nature of a sedimentary environment that had not completed the diagenetic process. The HMS ore zone carries the effects of post-mineralization processes between clastics and ore minerals. These fragments and ore minerals moved together during later processes to complete diagenesis and ore mineralization. The presence of banded ore in addition to snowball-like structures observed in metasedimentary units is a common textural feature of both clastics and ore sections Fig. 13c–d). These types of structure are associated with thrusting, folding and scouring of the sequence during transport from the pelagic environment onto the continent. Stockwork structures in the HMS ore zone are observed in the more limited area compared to

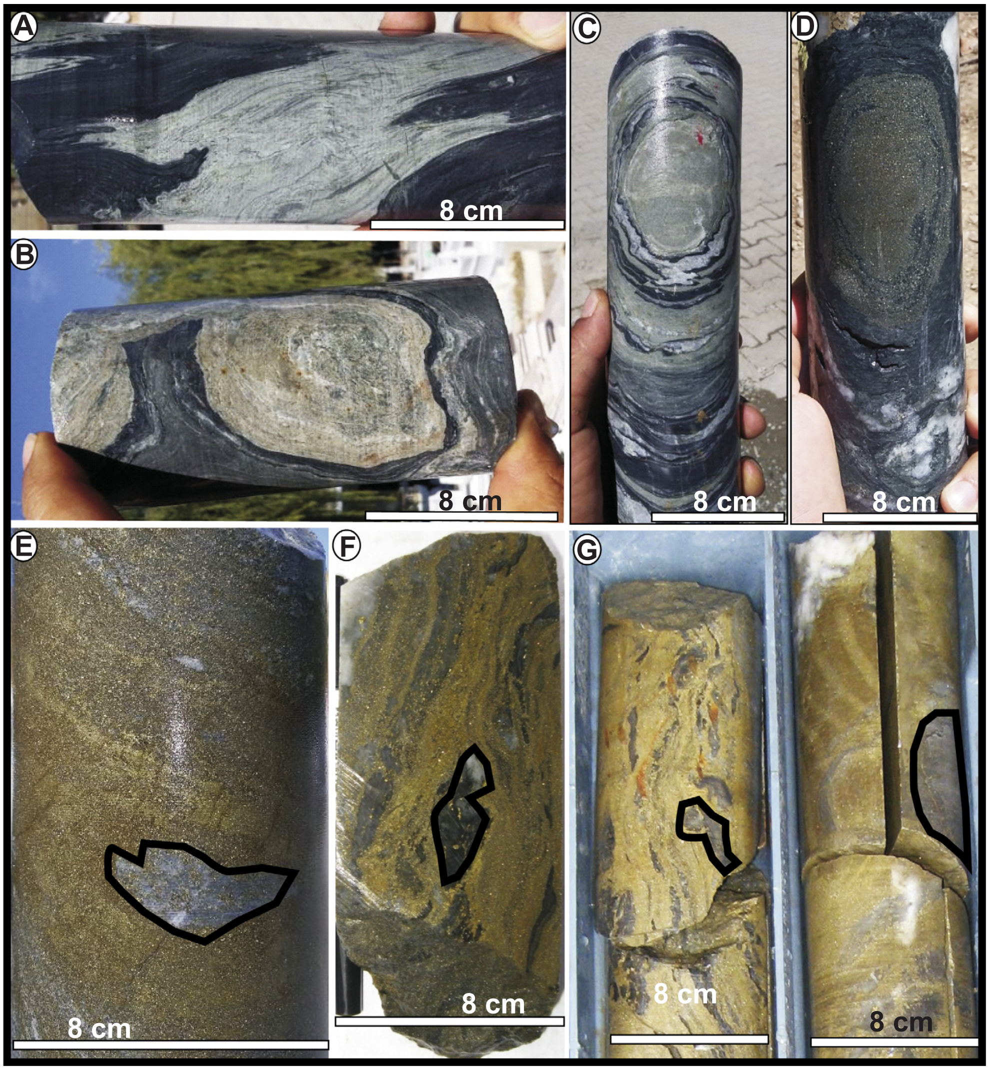

Fig. 13. Core photographs of wall rock and mineralizing system in HMS deposit. A-B- primary sedimentologic structures, C-D- snowball texture observed in wall rock and ore zones, E-G- mineralization-related replacement structures and siliceous clay relict phases.

disseminated-banded and massive ore. Additionally, no indications of a hydrothermal chimney were encountered related to massive ore. Within disseminated-banded and massive ore the presence of silicified zones surrounded by argillic sections developed during replacement processes (Fig. 14e–g).

The distinction of VMS mineralization style is linked to many criteria and knowledge of this situation is important for the exploration strategies. The basic criteria for mineralization style were classified by Tornos et al. (2015) as follows.

I- For mound-style mineralization: a mound or lens-shaped morphology; hydrothermal vent chimneys; widely distributed sulfide breccia; stratigraphic boundary control on the location of mineralization

II- For stratiform exhalative mineralization: sheet-like morphology developed before deformation; fine-grained host rocks, broad and planar stratification

III- For replacive mineralization: irregular geometry and distribution of sulfide mineralization; degrees of mineralization found; the presence of relict fragments in the host rock.

Geologic data obtained from the HMS ore system show that mineralization probably developed in the form of sub-seafloor replacement. Generally, volcanic and sedimentary layers are replaced by sulfides within feeder zones under exhalative mineralization (Tornos et al., 2015). However, there is no exhalative mound-style mineralization found associated with the HMS ore system. Massive ore levels within the HMS ore system appear as bands with varying thickness. Additionally, the observation of mineralization degrees (disseminated, massive/semi-massive sulfides), relict textures in host rock and irregular distribution of sulfide bodies are characteristics compatible with replacive mineralization.

6.3. Isotope signatures

The $\delta^{34}S$ data for pyrite and chalcopyrite vary within a fairly narrow range between +3.02‰ and +3.67‰, indicative of a fairly homogenous origin and formation conditions, the temperature in particular and also indicate the prevalent magmatic signature. Sulfur isotope data from the study area are comparable both with the other massive sulfide deposits of Turkey and the Besshi-type deposits occurring worldwide (Fig. 14). Although "deep-seated" sulfur may be a potential source for the deposits occurring in the area, a substantial input of seawater sulfate should also be considered since the most imperative source for sulfur in Phanerozoic VMS deposits is inorganically reduced seawater sulfate (Çağatay and Eastoe, 1995; Huston 1999; Gökce and Spiro, 2000; Revan et al., 2014). Lack of light-sulfur isotope enrichment may be due either to the non-existence of biogenic reduction of seawater

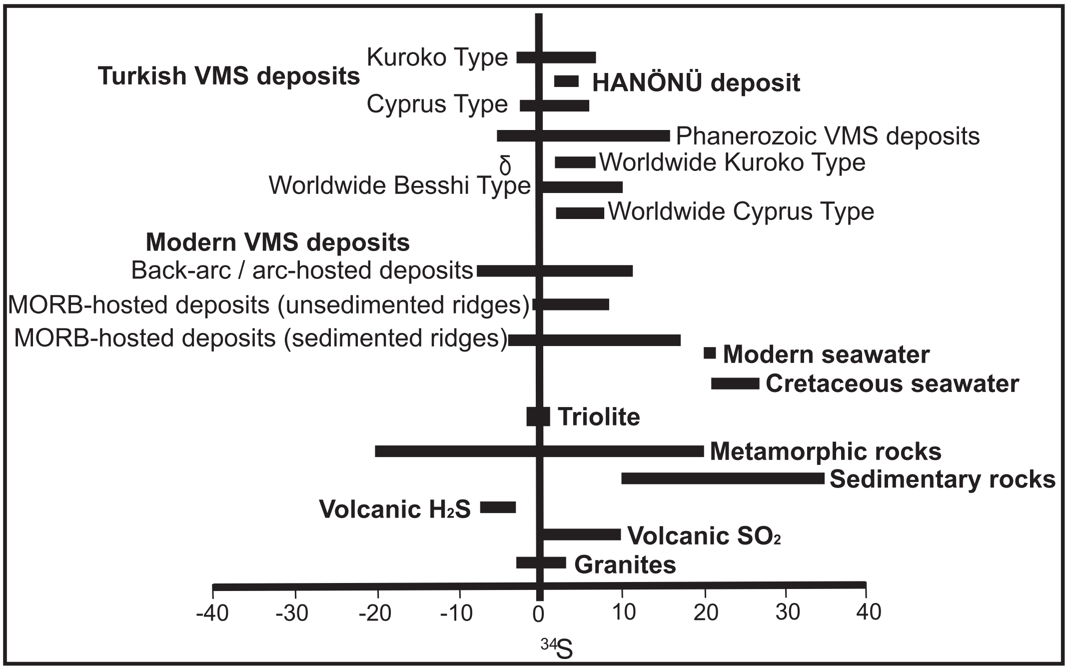

Fig. 14. The ranges of δ34S values of sulfides and sulfates associated with Kuroko-type VMS deposits and other VMS deposits in Turkey in comparison with other deposits and natural sulfur reservoirs (data from Ohmoto and Rye 1979; Arnold and Sheppard 1981; Kerridge et al., 1983; Zierenberg et al., 1984; Shanks and Seyfried, 1987; Woodruff and Shanks, 1988; Çağatay and Eastoe, 1995; Huston, 1999; Gökce and Spiro, 2000; Revan et al., 2014).

Table 4
206Pb/204Pb, 207Pb/204Pb and 208Pb/204Pb isotope ratios of sulfide ores from the Hanönü deposit.

Deposit	$^{206}Pb/^{204}Pb$ (± 2σ)	$^{207}Pb/^{204}Pb$ (± 2σ)	$^{208}Pb/^{204}Pb$ (± 2σ)
Hanonu1	18.416	15.561	38.07
Hanonu2	17.98	15.498	37.87
Hanonu3	18.233	15.539	38.009
Hanonu4	18.128	15.537	38.071
Hanonu5	18.091	15.538	38.034
Hanonu6	18.034	15.497	37.867
Hanonu7	18.042	15.525	38.002
Hanonu8	18.05	15.539	38.028

sulfate or that such a mechanism was subtle and/or locally effective (e.g. vent chimneys). Since vent chimney formations are not expected in this model of ore genesis, sulfur isotope data were considered to support the proposed model. Otherwise, there would be much broader $\delta^{34}S$ data (Ohmoto and Rye, 1979).

Lead isotope results (Table 4) acquired mainly from sulfide bulk samples consist mainly of pyrite and chalcopyrite for the major ore mineralization and are very similar with respect to their narrow compositional range and being less radiogenic. The data show a narrow range within the region indicating that the metal-transporting hydrothermal fluids were very homogeneous with respect to their lead isotope source. From the above lead isotope data, it is suggested that a large portion of the lead in the massive sulfide ores of the Hanönü area was sourced from igneous activity in an arc-related setting sourced by lower crust and upper mantle.

6.4. Tectonic setting and potential mineralization areas

Volcanogenic massive sulfide mineralization may have different submarine tectonic settings associated with arc-back-arc systems, in addition to oceanic and continental rifts (Hitzman et al., 2010). Apart from the sediment-hosted Hanönü massive sulfide deposit, there is massive sulfide mineralization with different genetic traits located in the Central and Eastern Pontides. In terms of time and space, there are three different types of VMS mineralization observed within the Pontide orogenic belt in Anatolian geography. The Küre massive sulfide deposit located northwest of this mineralization has been operating for ten years and is considered to be a Cyprus-type formation (Altun et al., 2015; Akbulut et al., 2016-Fig. 15A). This deposit is formed between basalts of the Küre ophiolite with tectonic contact with a flysch sequence and black shales, with lithologic control of well-developed mineralization with mound form and stockwork zones. Re-Os isotope data from ore related to the Küre sulfide mineralization indicate Jurassic age (180 Ma) (Akbulut et al., 2016). This age is compatible with regional-scale geologic results with the Küre basin developing as a back-arc basin in the Permian-early Jurassic (Akbulut et al., 2016). Comprehensive studies in recent years related to VMS mineralization in the Eastern Pontides (Çiftçi, 2000; Çiftçi et al., 2005; Eyüboğlu et al., 2014; Revan et al., 2014) have stated this mineralization developed related to the Early Campanian-Maastrichtian magmatic arc and called them Black Sea-type VMS deposits (Eyüboğlu et al., 2014; Fig. 15A). Dacites hosting Black Sea-type VMS mineralization are dated to the interval from 91.1 ± 1.3 to 82.6 ± 1 Ma and were formed by calc-alkaline and shoshonitic magma (Eyüboğlu et al., 2014). VMS deposits in the Eastern Pontides are associated with caldera-like depressions and dome-like structures in felsic magmas. The formation environment of these VMS deposits is reported to be intra-arc and near-arc regions of the Eastern Pontide orogenic belt (Eyüboğlu et al., 2014).

The geochemical characteristics of wall-rocks of the HMS mineralization, suggest that it probably formed in a basin behind an oceanic arc with mafic lava or sills/volcanoclastic lithology. The host rock of HMS mineralization is located within the Çangaldağ metamorphic complex, a Triassic-Jurassic allochthonous sequence in the Central Pontides. Studies in recent years have provided reliable data about the formation and metamorphism ages of rocks related to the Çangaldağ Metamorphic Complex (Okay et al., 2006; Aygül et al., 2015a, b; Çimen et al., 2016, 2017). Age data and geochemical characteristics of the Çangaldağ Metamorphic complex reveal a formation model related to a Middle Jurassic arc-back arc system for this complex (Çimen et al., 2016, 2017). Regional geologic data for HMS mineralization determine

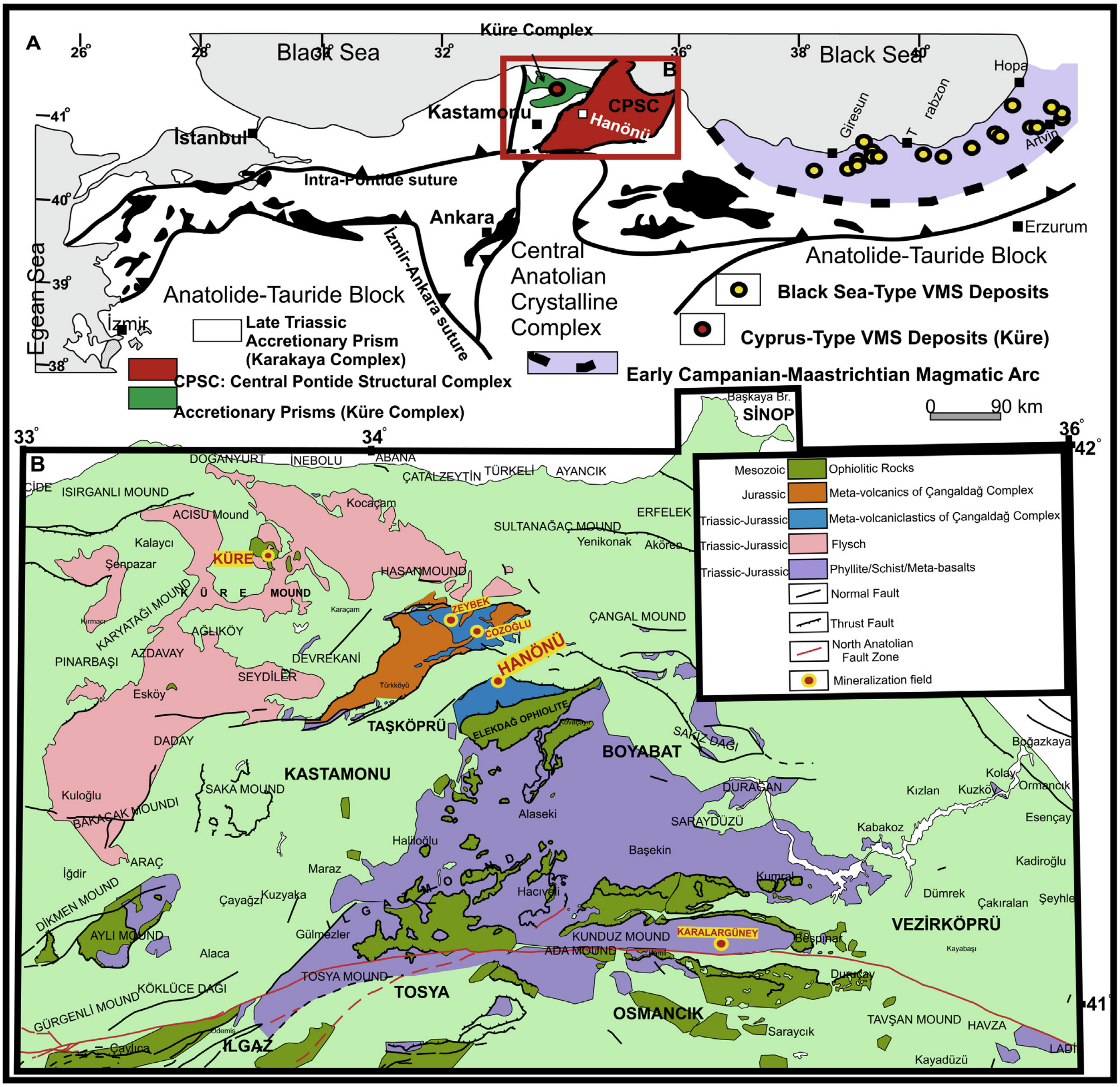

Fig. 15. A- Geologic map showing VMS mineralization and related rocks (Göncüoğlu, 2010; Eyüboğlu et al., 2014; Çimen et al., 2017). B- MTA 1/500,000 scale Sinop sheet geologic map .
adapted from Uğuz et al. (2002)

the common time and spatial features of the Küre and Çangaldağ metamorphic complexes. In light of geologic and geochemical data, HMS mineralization is related to the back-arc system mentioned above and formed simultaneously.

The CMC regionally developed associated with the intra-Pontide suture within the Central Pontide Structural Complex (Çimen et al., 2016, 2017, 2018). Areas with mafic-volcanoclastic lithologies within the complex form a target region for exploration of HMS-type mineralization. The Cozoğlu and Zeybek areas within the Çangaldağ Metamorphic complex contain HMS-type VMS mineralization discovered by our group with continuing studies. Additionally, on regional scale a potential area for VMS mineralization is formed by Triassic-Jurassic flysch sequence, and may be divided into three different units with northwest-southeast orientation (Fig. 15B). Located in the northwestern of HMS mineralization is a flysch unit with no metamorphism and unknown correlation to any back arc basic volcanism, with no findings related to VMS mineralization. As all identified VMS mineralization is associated with mafic volcanic rocks, VMS mineralization is not expected to develop within these flysch unit. Contrary to this, consist of the low metamorphism volcanoclastics and clastics within Çangaldağ metamorphic complex that host the HMS mineralization. Toward south of the region, meta flysch sequence with tectonic contact with the Elekdağ ophiolite that formed in a supra-subduction zone contains VMS mineralization findings. The ophiolite contacts in this sequence contain eclogite and amphibolite units. Additionally, the unit contains gabbro, andesite and limestone blocks displaying the character of a large accretionary melange. The sulfide mineralization identified in low degree metamorphic rocks in this sequence is similar to HMS-type mineralization. Exploration drilling by MTA in the Karalargüney area discovered an important region with very similar mineralization to HMS (see Fig. 15B). The Karalargüney VMS mineralization shows that HMS-type formations are found in the phyllite, schist and metabasalts units.

7. Conclusions

The HMS mineralization is hosted by metavolcanoclastics with mafic sills and/or lava intercalations in the Çangaldağ metamorphic complex (CMC) in the Central Pontides. Metamorphism in reaching greenschist facies and tectonic processes affected mineralization and all associated lithological units. The main mineral association of the HMS mineralization containing massive, banded and disseminated-banded sulfides is pyrite, chalcopyrite, sphalerite and minor magnetite. The HMS mineralization is dominantly Cu (0.2–6.9%) accompanied by Zn (239–10000 ppm). According to the base metal content, the mineralization is classified as Cu-Zn type of volcanogenic massive sulfide deposits. The geochemical features of mafic sills and/or lava interlayered with metavolcanoclastics indicate these rocks were derived from a source containing island arc components. The partial melting processes affecting source areas of basic rocks associated with mineralization were modeled. These partial melting models indicate the source of the mafic rocks associated with the HMS mineralization was a mixture of 70% depleted MORB mantle and 30% asthenospheric melt reaching 8–15% melting degree. Areas with this type of source lithology can be found in back-arc basins. The geochemical characteristics of clastic rocks related to the HMS ores indicate they were fed from rocks with oceanic crustal components and deposited in an associated basin. This data reveal that during HMS mineralization rifting was in a back-arc basin. Additionally, isotope data from the Hanönü massive sulfide mineralization indicate an arc-related environment with magmatic activity from the lower crust and upper mantle. The observation of varying degrees of HMS mineralization (disseminated-massive/semi-massive sulfides), relict textures from host rock in mineralization, and irregularity of sulfide body distribution shows that ore mineralization possibly developed through sub-seafloor replacement processes. The HMS mineralization is located within the Çangaldağ metamorphic complex, a Triassic-Jurassic allochthonous unit in the Central Pontides.

Acknowledgments

This study was completed as part of the "Kastamonu Province and surroundings Polymetallic Mineral Exploration" project numbered 2013-32-13-05 run by MTA (General Directorate of mineral research and exploration, Ankara, TURKEY). We wish to thank all MTA employees who contributed to the project and geological engineers Şenol Şahin, Serdar Keskin, Onur Tiryaki, Mustafa Mengeloğlu, Füsun Niğdeli and Levent Akduman who participated and contributed to the field studies of the project. We are grateful to Editor-in-Chief Prof. Franco Pirajno, Assoc. Editor Dr. İlkay KUŞÇU, Dr. Yener EYÜBOĞLU, Dr. David LENTZ and the manuscript reviewers for their constructive criticism and contributions.

Appendix A. Supplementary data

Supplementary data associated with this article can be found, in the online version, at https://doi.org/10.1016/j.oregeorev.2018.08.010. These data include Google maps of the most important areas described in this article.

References

Akbayram, K., Okay, A.I., Satır, M., 2012. Early Cretaceous closure of the Intra-Pontide Ocean in western Pontide (Northwestern Turkey). J. Geodyn. 65, 38–55.
Akbulut, M., Oyman, T., Çiçek, M., Selby, D., Özgenç, İ., Tokçaer, M., 2016. Petrography, mineral chemistry, fluid inclusion microthermometry and Re-Os geochronology of the Küre volcanogenic massive sulfide deposit (Central Pontides, Northern Turkey). Ore Geol. Rev. 76, 1–18.
Altun, Y., Yılmaz, H., Şiner, İ., Yazar, F., 2015. The secrets of massive sulfide deposits on mid-ocean ridge and Küre-Mağaradoruk copper deposit. Bull. Min. Res. Exp. 150, 51–65.
Arnold, M., Sheppard, S.M., 1981. East Pacific Rise at latitude 21 N: isotopic composition and origin of the hydrothermal sulphur. Earth Planet. Sci. Lett. 56, 148–156.
Aygül, M., Okay, A.I., Oberhansli, R., Ziemann, M.A., 2015a. Thermal structure of low-grade accreted Lower Cretaceous distal turbidites, the Central Pontides, Turkey: insights for tectonic thickening of an accretionary wedge. Turkish J Earth Sci 24, 461–474.
Aygül, M., Okay, A.I., Oberhansli, R., Schmidt, A., Sudo, M., 2015b. Late Cretaceous infant intra-oceanic arc volcanism, the Central Pontides, Turkey: petrogenetic and tectonic implications. https://doi.org/10.1016/j.jseaes.2015.07.005.
Barrett, T.J., Jarvis, I., Jarvis, K.E., 1990. Rare earth element geochem- istry of massive sulfides-sulfates and gossans on the southern Explorer Ridge. Geology 18, 583–586.
Barrie, C.T., Hannington, M.D., 1999. Classification of volcanic-associated massive sulfide deposits based on host rock composition. Rev. Econ. Geol. 8, 2–12.
Bhatia, M.R., Crook, K.A.W., 1986. Trace element characteristics of graywackes and tectonic setting discrimination of sedimenatry basins. Contrib. Miner. Petrol. 92, 181–193.
Bingöl, E., Akyürek, B., Korkmazer, B., 1975. Biga yarımadasının jeolojisi ve Karakaya Formasyonunun bazı özellikleri [The geology of the Biga Peninsula and some features of the Karakaya Formation]. Cumhuriyetin 50. Yılı Yerbilimleri Kongresi Tebliğleri, Maden Tetkik ve Arama Enstitüsü (MTA) Publications 70–77.
Boynton, W.V., 1984. Geochemistry of the rare earth elements: meteorite studies. In: Henderson, P. (Ed.), Rare Earth Element Geochemistry. Elsevier, pp. 63–114.
Bradshaw, G.D., Rowins, S.M., Peter, J.M., Taylor, B.E., 2003. Genesis of the Wolverine deposit, Finlayson Lake district, Yukon: a transitional style of polymetallic massive sulfide mineralization in an ancient continental margin setting. Gangue 1–7.
Brumsack, H.-J., 1989. Geochemistry of recent TOC-rich sediments from the Gulf of California and the Black Sea. Geol. Rundsch. 78, 851–882.
Catanzariti, R., Ellero, A., Göncüoğlu, M.C., Marroni, M., Ottria, G., Pandolfi, L., 2013. The Taraklı Flysch in the Boyali area (Sakarya Terrane, northern Turkey): implications for the tectonic history of the intraPontide suture zone. Compte Rendues des Geosciences 345, 454–461.
Cooper, J.R., Daasch, E.J., Kaye, M., 1974. Isotope and elemental geo- chemistry of Black Sea sediments. Am. Assoc. Pet. Geol. Mem. 20, 554–565.
Çağatay, M., Eastoe, C., 1995. A sulfur isotope study of volcanogenic massive sulfide deposits of the Eastern Black Sea province, Turkey. Miner. Deposita 30, 55–66.
Çiftçi, E., 2000. Mineralogy, paragenetic sequence, geochemistry and genesis of the gold and silver bearing Upper Cretaceous mineral deposits, northeastern Turkey. Ph.D. Dissertation. University of Missouri-Rolla, USA, pp. 251 (unpublished).
Çiftçi, E., Kolayli, H., Tokel, S., 2005. Lead-arsenic soil geochemical study as an exploration guide over the Killik volcanogenic massive sulfide deposit, Northeastern Turkey. J. Geochem. Explor. 86 (1), 49–59.
Çimen, O., Göncüoğlu, M.C., Sayit, K., 2016. Geochemistry of the metavolcanic rocks from the Çangaldağ Complex in the Central Pontides: implications for the Middle Jurassic arc-back-arc system in the Neotethyan Intra-Pontide Ocean. Turk. J. Earth Sci. 25, 491–512.
Çimen, O., Göncüoğlu, M.C., Simonetti, A., Sayit, K., 2017. Whole rock geochemistry, Zircon U-Pb and Hf isotope systematics of the Çangaldağ Pluton: evidences for Middle Jurassic Continental Arc Magmatism in the Central Pontides, Turkey. Lithos 290–291, 136–158.
Çimen, O., Göncüoğlu, M.C., Simonetti, A., Sayit, K., 2018. New zircon U-Pb LA-ICP-MS ages and Hf isotope data from the Central Pontides (Turkey): Geological and geodynamic constraints. J. Geodyn. 116, 23–36.
Doyle, M.G., Allen, R.L., 2003. Subsea-floor replacement in volcanic-hosted massive sulfide deposits. Ore Geol. Rev. 23, 183–222.
Doe, B.R., 1994. Zinc, copper, and lead in mid-ocean ridge basalts and the source rock control on Zn/Pb in ocean-ridge hydrothermal deposits. Geochim. Cosmochim. Acta 58, 2215–2223.
Eyüboğlu, Y., Santosh, M., Keewook, Yi., Tuysuz, N., Korkmaz, S., Akaryalı, E., Dudas, F. O., Bektaş, O., 2014. The Eastern Black Sea-type Volcanogenic Massive Sulfide Deposits: Geochemistry, zircon U-Pb geochronology and an overview of the geodynamics of ore genesis. https://doi.org/10.1016/j.oregeorev.2013.11.009.
Floyd, P.A., Winchester, J.A., 1978. Identification and discrimination of altered and metamorphosed volcanic rocks using immobile elements. Chem. Geol. 21, 291–306.
Fox, J.S., 1984. Besshi-type volcanogenic sulphide deposits - a review. Can. Inst. Min. Metall. Bull. 77 (864), 57–68.
Franklin, J.M., Lydon, J.W., Sangster, D.F., 1981. Volcanic-associated massive sulfide deposits. Econ. Geol., 75th Anniversary vol., 485–627.
Franklin, J.M., Gibson, H.L., Jonasson, I.R., Galley, A.G., 2005. Volcanogenic massive sulfide deposits. In: Hedenquist, J.W., Thompson, J.F.H., Goldfarb, R.J., Richards, J.P. (Eds.), Economic Geology—One Hundredth Anniversary Volume. Society of Economic Geol- ogists, Littleton, pp. 523–560.
Galley, A.G., Watkinson, D.H., Jonasson, I.R., Riverin, G., 1995. The subsea-floor formation of volcanic hosted massive sulfide: evidence from the Ansil deposit, Rouyn-Noranda, Canada. Econ. Geol. 90, 2006–2017.
Galley, A.G., Hannington, M.D., Jonasson, I.R., 2007. Volcanogenic mas- sive sulphide deposits: geological association of Canada. Mineral Deposits Division, Special Publication 5, 141–161.
Goodfellow, W.D., Blaise, B., 1988. Sulphide formation and hydrothermal alteration of hemipelagic sediments in Middle Valley, Northern Juan de Fuca Ridge. Can. Mineral. 26, 675–696.
Goodfellow, W.D., Franklin, J.M., 1993. Geology, mineralogy, and chemistry of sediment-hosted clastic massive sulfides in shallow cores, Middle Valley, Northern Juan de Fuca Ridge. Econ. Geol. 88, 2037–2068.
Goodfellow, W.D., McCutcheon, S.R., 2003. Geologic and genetic attributes of volcanic sediment-hosted massive sulfide deposits of the Bathurst Mining Camp, Northern New Brunswick—a synthesis. Econ. Geol. Monogr. 11, 245–301.
Goodfellow, W.D., Peter, J.M., 1996. Sulphur isotope composition of the Brunswick No. 12 massive sulphide deposit, Bathurst Mining Camp, N.B.: implications for ambient

environment, sulphur source, and ore genesis. Can. J. Earth Sci. 33, 231–251.
Goodfellow, W.D., Peter, J.M., Winchester, J.A., van Staal, C.R., 2003. Ambient marine environment and sediment provenance during formation of massive sulfide deposits in the Bathurst mining camp: importance of reduced bottom waters to sulfide precipitation and preservation. Econ. Geol. Monogr. 11, 129–156.
Gökce, A., Spiro, B., 2000. Sulfur-Isotope Characteristics of the Volcanogenic Cu-Zn-Pb Deposits of the Eastern Pontide Region, Northeastern Turkey. Int. Geol. Rev. 42 (6), 565–576.
Göncüoğlu, M.C., 2010. Introduction to the Geology of Turkey: geodynamic evolution of the pre-alpine and alpine terranes. General Directorate Min. Res. Exploration Monography Ser. 5, 69p.
Göncüoğlu, M.C., Kozlu, H., Dirik, K., 1997. Pre-Alpine and Alpine terranes in Turkey: explanatory notes to the terrane map of Turkey. Ann Geol Pays Helleniques 37, 515–536.
Göncüoğlu M.C., Turhan N., Sentürk K., Özcan A., Uysal S., 2000. A geotraverse across NW Turkey: tectonic units of the Central Sakarya region and their tectonic evolution. In: Bozkurt, E., Winchester, J.A., Piper, J.D. (Eds.), Tectonics and Magmatism in Turkey and the Surrounding Area. Geological Society of London Special Publication 173, London, UK, pp. 139–162.
Göncüoğlu, M.C., Gürsu, S., Tekin, U.K., Koksal, S., 2008. New data on the evolution of the Neotethyan oceanic branches in Turkey: Late Jurassic ridge spreading in the Intra-Pontide branch. Ofioliti 33, 153–164.
Göncüoğlu, M.C., Marroni, M., Pandolfi, L., Ellero, A., Ottria, G., Catanzariti, R., Sayit, K., 2014. The Arkot Dağ Mélange in Araç area, central Turkey: Evidence of its origin within the geodynamic evolution of the Intra- Pontide suture zone. J. Asian Earth Sci. 85, 117–139.
Göncüoğlu, M.C., Maroni, M., Sayit, K., Tekin, U.K., Ottria, G., Pandolfi, L., Ellero, A., 2012. The Ayli Dağ ophiolite sequence (central-northern Turkey): a fragment of middle Jurassic oceanic lithosphere within the Intra- Pontide suture zone. Ofioliti 37, 77–91.
Hamlyn, P.R., Keays, R.R., Cameron, W.E., Crawford, A.J., Waldron, H.M., 1985. Precious metals in magnesian low-Ti lavas: implications for metallogenesis and sülfür saturation in primary magmas. Geochim. Cosmochim. Acta 49, 1797–1811.
Hannington, M.D., Bleeker, W., Kjarsgaard, I., 1999. Sulfide mineralogy, geochemistry, and ore genesis of the Kidd Creek deposit: part II. The Bornite zone. Econ. Geol. Monogr. 10, 225–266.
Hart, W.K., Wolde, Gabriel G., Walter, R.C., Mertzman, S.A., 1989. Basaltic volcanism in Ethiopia: constraints on continental rifting and mantle interactions. J. Geophys. Res. 94, 7731–7748.
Herzig, P.M., Hannington, M.D., 1995. Polymetallic massive sulfides at the modern seafloor. A review. Ore Geol. Rev. 10, 95–115.
Hitzman, M.W., Selley, D., Bull, S., 2010. Formation of sedimentary rock-hosted stratiform copper deposits through earth history. Econ. Geol. 105, 627–639.
Hofmann, A.W., 1986. Nb in Hawaiian magmas: constraints on source composition and evolution. Chem. Geol. 57, 17–30.
Hofmann, A.W., 1988. Chemical differentiation of the Earth: the relationship between mantle, continental crust, and the oceanic crust. Earth Planet. Sci. Lett. 90, 297–314.
Hofmann, A.W., 1997. Mantle geochemistry: the message from oceanic volcanism. Nature 385, 219–229.
Humphris, S.E., Herzig, P.M., Miller, D.J., Alt, J.C., Becker, K., Brown, D., Brügmann, G., Chiba, H., Fouquet, Y., Gemmell, J.B., Guerin, G., Hannington, M.D., Holm, N.G., Honnorez, J.J., Itturino, G.J., Knott, R.L., Ludwig, R., Nakamura, K., Petersen, S., Reysenbach, A.L., Rona, P.A., Smith, S., Sturz, A.A., Tivey, M.K., Zhao, X., 1995. The internal structure of an active seafloor massive sulphide deposit. Nature 377, 713–716.
Huston, D.L., 1999. Stable isotopes and their significance for understanding the genesis of volcanic-hosted massive sulfide deposits: a review. Rev. Econ. Geol. 8, 157–179.
Hutchinson, R.W., 1973. Volcanogenic sulfide deposits and their metallogenic significance. Econ. Geol. 78, 1223–1246.
Keays, R.R., Scott, R.B., 1976. Precious metals in ocean-ridge basalts; implications for basalts as source rocks for gold mineralization. Econ. Geol. 71, 705–720.
Kerridge, J.F., Haymon, R.M., Kastner, M., 1983. Sulfur isotope systematics at the 21 N site, East Pacific Rise. Earth Planet. Sci. Lett. 66, 91–100.
Ketin, İ., 1966. Tectonic units of Anatolia (Asia Minor). Bull. Min. Res. Exp. 66, 23–34.
Klau, W., Large, D., 1980. Submarine exhalative Cu-Pb-Zn deposits. A discussion of their classification and metallogenesis. Geol. Jb. D40, 13–58.
Krienitz, M.S., Haase, K.M., Mezger, K., Eckardt, V., Shaikh-Mashail, M.A., 2006. Magma genesis and crustal contamination of continental intraplate lavas in northwestern Syria. Contrib. Mineral. Petrol. 151, 698–716.
Large, R.R., 1992. Australian volcanic-hosted massive sulfide deposits; features, styles, and genetic models. Econ. Geol. 87 (3), 471–510.
Lee, Y.I., 2002. Provenance derived from the geochemistry of late Paleozoic-early Mesozoic mudrocks of the Pyeongan Supergroup, Korea. Sed. Geol. 149, 219–235.
Leybourne, M.I., Goodfellow, W.D., 1994. Mineralogy and mineral chemistry of hydrothermally altered sediment, Middle Valley, Juan de Fuca Ridge. Proc. Ocean Drilling Program, Scientific Results 139, 155–206.
Liu, Y.-G., Miah, M.R.U., Schmitt, R.A., 1988. Cerium: a chemical tracer for paleo-oceanic redox conditions. Geochimica et Cosmochimica Acta 52, 1361–1371.
Lustrino, M., Wilson, M., 2007. The circum-Mediterranean anorogenic Cenozoic igneous province. Earth-Sci. Rev. 81, 1–65.
Lydon, J.W., 1984. Volcanogenic massive sulphide deposits, Part 1-A descriptive model. Geosci. Can. 11, 195–202.
McKenzie, D.P., O'Nions, R.K., 1991. Partial melt distributions from inversion of rare earth element concentrations. J. Petrol. 32, 1021–1091.
McLennan, S.M., 1989. Rare earth elements in sedimentary rocks: influence of provenance and sedimentary processes. Rev. Mineral. 21, 169–200.
Michard, A., Albarede, F., Michard, G., Minster, J.F., Charlou, J.L., 1983. Rare-earth elements and uranium in high-temperature solutions from East Pacific Rise hydrothermal vent field (13°N). Nature 303, 795–797.
Mosier, D.L., Singer, D.A., Salem, B.B., 1983. Geologic and grade-tonnage information on volcanic-hosted copper-zinc-lead massive sulphide deposits. U.S. Geological Survey Open-File Report 77, 83–89.
Nesbitt, H.W., Young, G.M., 1982. Early Proterozoic climates and plate motions inferred from major element chemistry of lutites. Nature 299, 715–717.
Nozaki, T., Kato, Y., Suzuki, K., 2013. Late Jurassic ocean anoxic event: evidence from voluminous sulphide deposition and preservation in the Panthalassa. Sci. Report 3 (1889), 1–6.
Ohmoto, H.H., 1996. Formation of volcanogenic massive sulfide deposits: the Kuroko perspective. Ore Geol. Rev. 10, 135–177.
Ohmoto, H., Rye, R.O., 1979. Isotopes of sulfur and carbon. Geochemistry of hydrothermal ore deposits. In: Barnes, H.L. (Ed.), Geochemistry of Hydrothermal Ore Deposits, second ed. Wiley, New York, pp. 509–567.
Okay, A.I., Tüysüz, O., 1999. Tethyan sutures of northern Turkey. In: Durand, B., Jolivet, L., Horváth, F., Séranne, M. (Eds.), The Mediterranean Basins: Tertiary Extension with the Alpine Orogen. Geological Society, London, Special Publication 156, pp. 475–515.
Okay, A.I., Göncüoglu, M.C., 2004. The Karakaya Complex: a review of data and concepts. Turk. J. Earth Sci. 13, 77–95.
Okay, A.I., Tüysü, Z.O., Satır, M., Özkan-Altıner, S., Altıner, D., Sherlock, S., Eren, R.H., 2006. Cretaceous and Triassic subduction-accretion, high-pressure-low-temperature metamorphism, and continental growth in the Central Pontides, Turkey. GSA Bul. 118, 1247–1269.
Okay, A.I., Gürsel, S., Sherlock, S., Altıner, D., Tüysüz, O., Kylander-Clark, A.R.C., Aygül, M., 2013. Early Cretaceous sedimentation and orogeny on the active margin of Eurasia: Southern Central Pontides, Turkey. Tectonics 32, 1247–1271.
Okay, A.I., Gürsel, S., Tüysüz, O., Sherlock, S., Keskin, M., Kylander-Clark, A.R.C., 2014. Low-pressure - high-temperature metamorphism during extension in a Jurassic magmatic arc, Central Pontides, Turkey. J. Metamorph. Geol. 32, 49–69.
Pearce, J.A., Cann, J.R., 1973. Tectonic setting of basic volcanic rocks determined using trace element analyses. Earth Planet. Sci. Lett. 19, 290–300.
Pearce, J.A., Parkinson, I.J., 1993. Trace element models for mantle melting: application to volcanic arc petrogenesis. In: Prichard, H. M., Alabaster, T., Harris, N.B.W., Neary, C.R. (Eds.), Magmatic Processes and Plate Tectonics. Geological Society, London, Special Publications 76, pp. 373–403.
Peter, Jan M., Scott, Steven D., 1999. Windy Craggy, Northwestern British Columbia: The world's largest Besshi-type deposit. Rev. Econ. Geol. 8, 261–296.
Peters, T.J., Menzies, M., Thirlwall, M., Kyle, P., 2008. Zuni-Bandera volcanism, Rio Grande, USA – melt formation in garnet- and spinel-facies mantle straddling the asthenosphere-lithosphere boundary. Lithos 102, 295–315.
Peltonen, P., Kontinen, A., Hhma, H., Kuronen, U., 2007. New mineral deposit model for the Cu-Co-Zn-Ni-Ag-Au sulphide deposits in Outukumpu, Finland. SGA News 21, 1–9.
Piercey, S.J., 2011. The setting, style, and role of magmatism in the formation of volcanogenic massive sulfide deposits. Mineral. Deposita 46, 449–471.
Pirajno, F., Jones, J.A., Hocking, R.M., Halilovic, J., 2004. Geology and tectonic evolution of Palaeoproterozoic basins of the eastern Capricorn Orogen, Western Australia. Precambr. Res. 128, 315–342.
Pirajno, F., 2009. Hydrothermal Processes and Mineral Systems. Springer, Berlin, pp. 1250.
Pirajno, F., Chen, Y., Li, N., Li, C., Zhou, L., 2016. Besshi-type mineral systems in the Palaeoproterozoic Bryah Rift-Basin, Capricorn Orogen, Western Australia: implications for tectonic setting and geodynamic evolution. Geosci. Front. 7, 345–357.
Plank, T., Langmuir, C.H., 1998. The chemical composition of subducting sediment and its consequences for the crust and mantle. Chem. Geol. 145, 325–394.
Revan, M.K., Genç, Y., Maslennikov, V.V., Maslennikova, S.P., Large, R.R., Danyushevsky, L.V., 2014. Mineralogy and trace-element geochemistry of sulfide minerals in hydrothermal chimneys from the Upper-Cretaceous VMS deposits of the Eastern Pontide orogenic belt (NE Turkey). Ore Geol. Rev. 63, 129–149.
Robertson, A.H.F., 2002. Overview of the genesis and emplacement of Mesozoic ophiolites in the Eastern Mediterranean Tethyan region. Lithos 65, 1–67.
Robertson, A.H., Ustaömer, T., 2004. Tectonic Evolution Of The Intra-Pontide Suture Zone In The Armutlu Peninsula, Nw Turkey. Tectonophysıcs 381, 175–209.
Saunders, A.D., Storey, M., Kent, R.W., Norry, M.J., 1992. Consequences of plume-lithosphere interactions: In: Storey, B.C., Alabaster, T., Pankhurst, R.J. (Eds.), Magmatism and the Causes of Continental Break-up: Geological Society. London, Special Publications, 68, pp. 41–60.
Sawkins, F.J., 1976. Massive sulphide deposits in relation to geotectonics. Geol. Assoc Can Spec. Pap. 14, 221–240.
Scott, S.D., 1992. Polymetallic sulfide riches from the deep: fact or fallacy? In: Hsu, K.J., Thiede, J. (Eds.), Use and Misuse of the Seafloor. Wiley & Sons, New York, pp. 87–115.
Shanks, W.C., Seyfried, W.E., 1987. Stable isotope studies of vent fluids and chimney minerals, southern Juan de Fuca Ridge: sodium metasomatism and seawater sulfate reduction. J. Geophys. Res. Solid Earth 92 (B11), 11387–11399.
Shaw, D.M., 1970. Trace element fractionation during anatexis. Geochim. Cosmochim. Acta 34, 237–243.
Shaw, J.E., Baker, J.A., Menzies, M.A., Thirlwall, M.F., İbrahim, K.M., 2003. Petrogenesis of the largest intraplate volcanic field on the Arabian Plate (Jordan): a mixed lithosphere–asthenosphere source activated by lithospheric extension. J. Petrol. 44, 1657–1679.
Shervais, M., 1982. Ti–V plots and the petrogenesis of modern and ophiolitic lavas. Earth Planet. Sci. Lett. 59, 101–118.
Solomon, M., 1976. Volcanic massive sulphide deposits and their host rocks — a review

and explanation. In: Wolf, K.H. (Ed.), Handbook of Stratabound and Stratiform Ore Deposits. Elsevier, Amsterdam, pp. 21–54.
Solomon, M., Gemmell, J.B., Zaw, K., 2004a. Nature and origin of the fluids responsible for forming the Hellyer Zn–Pb–Cu, volcanic-hosted massive sulphide deposit, Tasmania, using fluid inclusions, and stable and radiogenic isotopes. Ore Geol. Rev. 25, 89–124.
Solomon, M., Tornos, F., Large, R.R., Badham, J.N.P., Both, R.A., Zaw, K., 2004b. Zn–Pb–Cu volcanic-hosted massive sulphide deposits: criteria for distinguishing brine pool—from black smoker-type sulphide deposition. Ore Geol. Rev. 25, 259–284.
Sun, S.S., McDonough, W.F., 1989. Chemical and isotopic systematics of oceanic basalts: implications for mantle composition and processes. In: Saunders, A.D., Norry, M.J. (Eds.), Magmatism in the Ocean Basins. Geological Society of London, Special Publication, 42, pp. 45–313.
Sverjensky, D.A., 1984. Europium redox equilibria in aqueous solution. Earth Planet. Sci. Lett. 67, 70–78.
Şengör, A.M.C., Yılmaz, Y., 1981. Thethyan evolution of Turkey: a plate tectonics approach. Tectonophysics 75, 181–241.
Taylor, S.R., McLennan, S.M., 1985. The continental crust: its composition and evolution, Geoscience Texts. Blackwell Scientific Publications, London.
Tekeli, O., 1981. Subduction complex of pre-Jurassic age, northern Anatolia, Turkey. Geology 9, 68–72.
Thirlwall, M.F., Upton, B.G.J., Jenkins, C., 1994. Interaction between continental lithosphere and the Iceland plume-Sr–Nd–Pb isotope geochemistry of Tertiary basalts, NE Greenland. J. Petrol. 35, 839–879.
Tornos, F., 2006. Environment of formation and styles of volcanogenic massive sulfides: the Iberian Pyrite Belt. Ore Geol. Rev. 28, 259–307.
Tornos, F., Solomon, M., Conde, C., Spiro, B.F., 2008. Formation of the Tharsis massive sulfide deposit, Iberian Pyrite Belt: geological, lithogeochemical, and stable isotope evidence for deposition in a brine pool. Econ. Geol. 103, 185–214.
Tornos, F., Peter, I.J.M., Allen, R., Conde, C., 2015. Controls on the siting and style of volcanogenic massive sulphide deposits. Ore Geol. Rev. 68, 142–163.
Uğuz, M.F., Sevin, M., Duru, M., 2002. 1:500.000 ölçekli Türkiye Jeoloji Haritaları Sinop Paftası: MTA Gen. Md., Ankara.
Ustaömer, T., Robertson, A.H.F., 1999. Geochemical evidence used to test alternative plate tectonic models for pre-Upper Jurassic (Palaeotethyan) units in the Central Pontides. N Geol. J. 34, 25–53.
Ustaömer, T., Robertson, A.H.F., 1997. Tectonic–sedimentary evolution of the north Tethyan margin in the central Pontides of northern Turkey. In: Robinson, A.G. (Ed.), Regional and Petroleum Geology of the Black Sea and Surrounding Region. American Association of Petroleum Geologists Memoir 68, pp. 255–290.
Vine, J.D., Tourtelot, E.B., 1970. Geochemistry of black shale deposits—a summary report. Economıc Geology 65, 253–272.
Wang, K.L., Chung, S., O'Reilly, S.Y., Sun, S., Shinjo, R., Chen, C., 2004. Geochemical Constraints for the Genesis of Post-collisional Magmatism and the Geodynamic Evolution of the Northern Taiwan Region. J. Petrol. 45, 975–1011.
Winchester, J.A., Floyd, P.A., 1977. Geochemical discrimination of different magma series and their differentiation products using immobile elements. Chem. Geol. 20, 325–343.
Wood, D.A., 1980. The application of a Th–Hf/Ta diagram to problems of tectonomagmatic classification and to establishing the nature of crustal contamination of basaltic lavas of the British Tertiary volcanic province. Earth Planet. Sci. Lett. 50, 11–30.
Wolf, R., Anders, E., 1980. Moon and Earth: compositional differences inferred from siderophiles, volatiles, and alkalis in basalts. Geochim. Cosmochim. Acta 44, 2111–2124.
Woodruff, L.G., Shanks, W.C., 1988. Sulfur isotope study of chimney minerals and vent fluids from 21 N, East Pacific Rise: Hydrothermal sulfur sources and disequilibrium sulfate reduction. J. Geophys. Res. Solid Earth 93 (B5), 4562–4572.
Workman, R.K., Hart, S.R., 2005. Major and trace element composition of the depleted MORB mantle (DMM). Earth Planet. Sci. Lett. 231, 53–72.
Yılmaz, Y., Şengör, A.M.C., 1985. Palaeo-Tethyan ophiolites in northern Turkey: petrology and tectonic setting. Ofioliti 10, 485–504.
Zierenberg, R.A., Shanks, W.C., Bischoff, J.L., 1984. Massive sulfide deposits at 21 N, East Pacific Rise chemical composition, stable isotopes, and phase equilibria. Geol. Soc. Am. Bull. 95 (8), 922–929.